From:	Hannah Marie Horowitz
To:	UTC DL Records Center
Subject:	Comment on dockets UE-160918 and UG-160919
Date:	Thursday, February 22, 2018 12:13:46 AM
Attachments:	Kort_et_al-2016-Geophysical_Research_Letters.pdf Reversal of global atmospheric ethane and propane trends largely due to US oil and natural gas production _ Nature Geoscience.pdf

Hello. My name is Hannah Horowitz. Thank you for this opportunity to comment on Dockets UE-160918 and UG-160919. I am currently a postdoctoral researcher at the University of Washington after completing my PhD in atmospheric chemistry at Harvard University. In graduate school, my research focused on understanding mercury pollution, which is toxic and can harm our cardiovascular and nervous systems. In the US, coal-fired power plants are the number one source of mercury emissions. Because of this and other air-quality improvements that will further benefit human health, I applaud Puget Sound Energy for making a commitment to close two of its units at the Colstrip coal plant - and urge PSE to transition from coal entirely.

As an atmospheric chemist, I am deeply concerned by natural gas production from unconventional resources, like shale gas or fracked gas. Leaks of methane, a more powerful heat-trapping gas than CO_2, can erase any efficiency benefits of natural gas. In addition, leaks of methane and more importantly ethane worsen regional ozone air quality. Ozone irritates our lungs, triggers asthma attacks, and also leads to costly damages to crops. US shale oil and gas production alone is largely why globally ethane levels have started increasing. More ethane can even lengthen the time that methane remains in the atmosphere, further compounding global warming.

My current research now focuses on understanding impacts of climate change. I was inspired by my final class in graduate school, called "consequences of energy systems". Our final project was figuring out how to reach US greenhouse gas reduction targets by 2050. Turns out, it's nearly impossible. I realized we needed all hands on deck. Decarbonization of our energy production is essential and requires creative solutions. PSE has a choice to make – to be an innovative leader or to lag behind by extracting and burning natural gas, releasing the powerful heat-trapping methane in the process.

Thank you again. I am attaching two relevant studies from scientific peer-

reviewed journals.

Hannah Horowitz
Seattle, WA

AGU PUBLICATIONS

Geophysical Research Letters

RESEARCH LETTER
10.1002/2016GL068703

Key Points:
- The Bakken shale in North Dakota accounted for 1–3% total global ethane emissions in 2014
- These findings highlight the importance of shale production in global atmospheric ethane shift
- These emissions impact air quality and influence interpretations of recent global methane changes

Supporting Information:
- Supporting Information S1
- Movie S1

Correspondence to:
E. A. Kort,
eakort@umich.edu

Citation:
Kort, E. A., M. L. Smith, L. T. Murray, A. Gvakharia, A. R. Brandt, J. Peischl, T. B. Ryerson, C. Sweeney, and K. Travis (2016), Fugitive emissions from the Bakken shale illustrate role of shale production in global ethane shift, *Geophys. Res. Lett.*, *43*, 4617–4623, doi:10.1002/2016GL068703.

Received 22 JAN 2016
Accepted 12 APR 2016
Accepted article online 26 APR 2016
Published online 7 MAY 2016

Fugitive emissions from the Bakken shale illustrate role of shale production in global ethane shift

E. A. Kort[1], M. L. Smith[1], L. T. Murray[2,3], A. Gvakharia[1], A. R. Brandt[4], J. Peischl[5,6], T. B. Ryerson[5], C. Sweeney[5,6], and K. Travis[7]

[1]Climate and Space Sciences and Engineering, University of Michigan, Ann Arbor, Michigan, USA, [2]NASA Goddard Institute for Space Studies, New York, New York, USA, [3]Lamont-Doherty Earth Observatory, Columbia University, Palisades, New York, USA, [4]Department of Energy Resources Engineering, Stanford University, Stanford, California, USA, [5]NOAA Earth System Research Laboratory, Boulder, Colorado, USA, [6]Cooperative Institute for Research in Environmental Science, University of Colorado Boulder, Boulder, Colorado, USA, [7]Department of Earth and Planetary Science, Harvard University, Cambridge, Massachusetts, USA

Abstract Ethane is the second most abundant atmospheric hydrocarbon, exerts a strong influence on tropospheric ozone, and reduces the atmosphere's oxidative capacity. Global observations showed declining ethane abundances from 1984 to 2010, while a regional measurement indicated increasing levels since 2009, with the reason for this subject to speculation. The Bakken shale is an oil and gas-producing formation centered in North Dakota that experienced a rapid increase in production beginning in 2010. We use airborne data collected over the North Dakota portion of the Bakken shale in 2014 to calculate ethane emissions of 0.23 ± 0.07 (2σ) Tg/yr, equivalent to 1–3% of total global sources. Emissions of this magnitude impact air quality via concurrent increases in tropospheric ozone. This recently developed large ethane source from one location illustrates the key role of shale oil and gas production in rising global ethane levels.

1. Introduction

Fossil fuels are the primary source of ethane (C_2H_6) to the atmosphere due to emissions during extraction, processing, and distribution [*Blake and Rowland*, 1986; *Rudolph*, 1995; *Xiao et al.*, 2008; *Simpson et al.*, 2012]. Additional sources include biofuels, biomass burning, and smaller contributions from biogenic and geologic sources [*Etiope and Ciccioli*, 2009]. The atmospheric abundance of ethane results from a balance between emissions and removal via reaction with the hydroxyl radical (OH). This reaction consumes OH, reducing atmospheric oxidative capacity and, depending on the chemical environment, can subsequently worsen air quality by enhancing tropospheric ozone (O_3) formation through multiple pathways [*Aikin et al.*, 1982]. Ethane's consumption of OH also increases the atmospheric lifetime of methane (CH_4). Ethane thus acts as both a direct and indirect (via O_3 and CH_4) greenhouse gas, with modest global impact [*Highwood et al.*, 1999; *Collins et al.*, 2002]. The lifetime of ethane in the atmosphere is ~2 months, though it strongly varies seasonally at middle and high latitudes [*Goldstein et al.*, 1995]. Concentrations in the remote atmosphere typically range from less than 1 ppb to 2 ppb [*Simpson et al.*, 2012], with much higher levels encountered in the vicinity of sources [*Smith et al.*, 2015]. Total global emissions are estimated at 11.3 Tg C_2H_6/yr in 2010 [*Simpson et al.*, 2012]. While global observations suggest that emissions declined from 1984 to 2010 (14.3 to 11.3 Tg/yr), one remote mountaintop location in Europe reported an increase in regional atmospheric levels suggesting increased emissions again from 2009 [*Franco et al.*, 2015]. While the decline in ethane emissions was attributed to reduced fossil fuel sources [*Simpson et al.*, 2012], the more recent increase since 2009 was hypothesized to possibly be caused by the increase in shale gas production in the U.S., though without observations made in the U.S. [*Franco et al.*, 2015].

The idea that the U.S. shale gas contribution is responsible for the recent global increase in ethane is plausible given the rapid increase in U.S. oil and gas production in the past decade. Much attention from the public and atmospheric community has focused on the greenhouse gas impacts of expanding shale gas production [*Brandt et al.*, 2014; *Peischl et al.*, 2015; *Karion et al.*, 2015; *Caulton et al.*, 2014], whereas the rapid increase in shale oil production has received less attention. The Bakken Formation of western North Dakota, primarily an oil-producing region where natural gas is a by-product, has seen substantial increases over the last decade with production levels in 2014 exceeding 2005 by a factor in excess of 3500 for oil and 180 for gas (Figure 1,

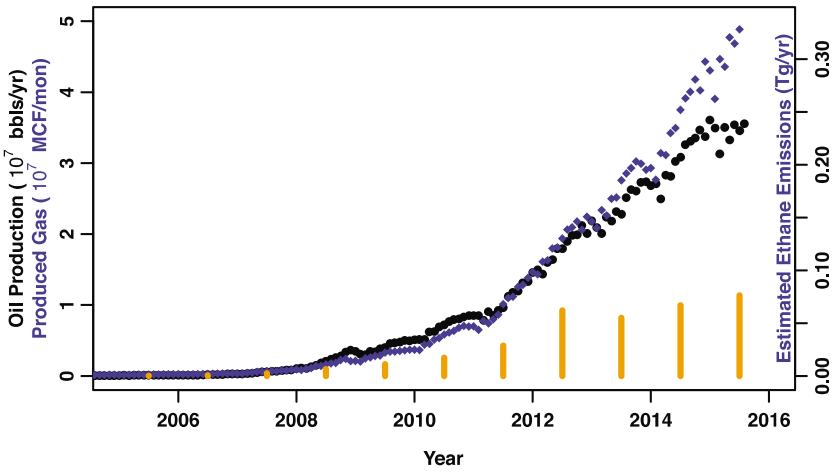

Figure 1. Oil (black circles) and gas (blue diamonds) production and estimated emissions (blue) and estimated emissions growth rate (orange) for the Bakken Shale in North Dakota. Production data from the North Dakota Department of Mineral Resources. On the right axis we show estimated ethane emission assuming the emissions rate observed in 2014 scales linearly with natural gas production. Emissions growth rate is shown in orange. Notice the very large increase in production (and likely emissions) since 2010.

North Dakota Department of Mineral Resources). This tremendous increase in productivity has the potential to significantly impact the atmosphere if hydrocarbons are leaked or vented to the atmosphere prior to combustion. Here we present and analyze observations collected over the North Dakota portion of the Bakken shale during a National Oceanic and Atmospheric Administration (NOAA) airborne study conducted in Spring of 2014.

2. Materials and Methods

2.1. Aircraft Flights and Instrumentation

Flights were conducted in May 2014 with the National Oceanic and Atmospheric Administration (NOAA) DHC-6 Twin Otter aircraft. This study focused on assessing the atmospheric impact of oil and gas production in the Bakken with continuous measurements of methane, ethane, carbon dioxide, water vapor, carbon monoxide, ozone, black carbon, wind, pressure, and temperature as well as whole-air flask samples for analysis of dozens of other compounds. Flights consisted of horizontal transects in the daytime boundary layer to characterize emissions from the entire Bakken field, along with vertical profiles to quantify the depth of the mixed layer. The Twin Otter flew on 12 separate days. Flights typically were 3 to 3.5 h; on half of the flight days two research flights were flown (one 3–3.5 h flight, a stop for refueling, and then a second 3–3.5 h flight). Four different days (of the 12 research flight days) with steady winds appropriate for mass balance calculations are the focus of the analysis where we analyze downwind flights characterizing emissions from the entire field.

Airborne ethane measurements were made with an Aerodyne mini direct absorption spectrometer. The instrument has been described in detail previously [*Smith et al*., 2015; *Yacovitch et al*., 2014]. The instrument was deployed as in *Smith et al*. [2015] with the addition of hourly sampling of a standard gas to verify instrument stability. The instrument scans multiple ethane absorption lines centered at 3.3 μm. Air is not dried prior to sampling; wet air mole fractions are observed and converted to dry mole fraction (values reported here) using the coincident water vapor observation made by a Picarro G2401-m. In-flight precision in typical conditions was < 0.1 ppb. Assessment of in-flight standards indicates accuracy averages 0.5 ppb. All data reported here are dry air molar fraction, adjusted to be on the NOAA-2012 ethane scale by precampaign and postcampaign calibration (standard gas cylinders were prepared gravimetrically). Airborne methane measurements were made with a Picarro G2401-m. Sampling frequency is ~0.5 Hz. In-flight calibrations ensure reported dry air mole fraction is on the World Meteorological Organization X2004A scale [*Dlugokencky et al*., 2005]. Total uncertainty is estimated at ±1.0 ppb. Wind speed and direction were measured at 1 Hz with estimated uncertainty at ±1 m/s with a differential GPS approach as described by *Conley et al*. [2014]. Ozone was measured with a 2B Technologies analyzer. A Rosemount deiced total temperature

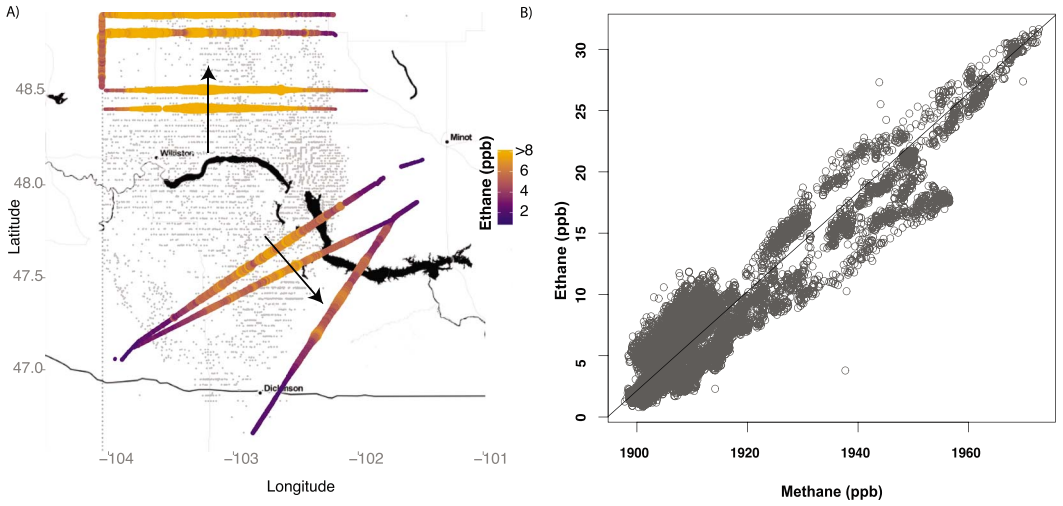

Figure 2. Ethane and methane observations over the Bakken Shale. (a) Mass balance flight tracks colored by C_2H_6 for 13, 14, 21, and 22 May 2014. Approximate winds illustrated, from the NW for 13 and 14 May (flight paths below 48°), and S to SW for 21 and 22 May (flight paths above 48° have been shifted for visual clarity). The locations of gas-producing wells are shown in gray dots. (b) C_2H_6:CH_4 from legs illustrated in Figure 2a, exhibiting a slope of 40.5% (95% CI 40.2 to 40.7) as calculated accounting for variance in both CH_4 and C_2H_6 using a ranged major axis regression [*Legendre and Legendre*, 1998]. This closely matches the 42% C_2H_6:CH_4 ratio present in raw gas.

sensor, model 102CP2AF, was used to measure ambient temperature. This was calibrated before and after the campaign and performed with estimated precision of ±0.2°C and accuracy of ±1.0°C.

2.2. Mass Balance Methodology

The mass balance approach provides an observation-based method for quantifying atmospheric fluxes of trace gases from a defined area. This approach assumes steady horizontal wind fields and a well-developed planetary boundary layer (PBL). We apply this method as has been extensively documented and demonstrated in the past for similar studies of oil- and gas-producing basins for methane, ethane, and black carbon [*Smith et al.*, 2015; *Peischl et al.*, 2015; *Karion et al.*, 2013, 2015; *Petron et al.*, 2014; *Schwarz et al.*, 2015]. The ethane flux is calculated as follows:

$$\mathrm{flux}_{\mathrm{ethane}} = v\int_{-b}^{b} X_{\mathrm{ethane}} \int_{z_{\mathrm{ground}}}^{z_1} n_{\mathrm{air}}\,\mathrm{d}z \quad \cos(\theta)\mathrm{d}x$$

Here X_{ethane} is the molar enrichment of ethane above background concentrations, $v\cos(\theta)$ is the component of the horizontal wind perpendicular to the flight path, $-b$ to b is the width of the downwind plume, n_{air} is the molar mass of dry air, z_{ground} is the ground level of the flight leg, and z_1 represents the top of the mixing box. We calculate z_1 as described by *Peischl et al.* [2015], where we account for ethane enhancements just above the PBL top by increasing the integrated mixing depth.

$$z_1 = \left(3z_{\mathrm{pbl}} + z_e\right)/4$$

where z_{pbl} is defined as the top of the well-mixed layer and z_e is the top of the entrainment zone. This adjustment has a minimal impact in the study considered here. On average z_1 is ~6% larger than z_{pbl}.

3. Observations and Ethane Flux Estimate

The atmospheric C_2H_6:CH_4 relationship observed over and downwind of the Bakken shale was consistent and elevated throughout the campaign. On downwind flight legs characterizing the total field emissions (Figure 2 a), we observed a 40.5% molar C_2H_6:CH_4 enhancement ratio (95% confidence interval (CI) 40.2 to 40.7; Figure 2b). This is a notably higher value than observed over Los Angeles [*Wennberg et al.*, 2012; *Peischl et al.*, 2013] or over the Barnett shale in Texas [*Smith et al.*, 2015], where molar enhancement ratios tended to remain below 15%. This very high C_2H_6:CH_4 enhancement ratio in the Bakken is consistent with an oil-bearing

Table 1. Average Molar Composition of Natural Gas in the Bakken Shale (Means Normalized to 100%) as Reported in *Brandt et al.* [2015][a]

C_1	C_2	C_3	iC_4	nC_4	iC_5	nC_5	C_6	O_2/Ar	CO_2	N_2	H_2S
47.0	19.8	14.0	1.6	4.7	0.8	1.3	1.7	0.1	1.2	7.5	0.2

[a]This corresponds to an ethane:methane (C_2:C_1) molar ratio of 42%.

reservoir rich in higher hydrocarbons and exhibiting a C_2H_6:CH_4 ratio of 42% based on 710 reported below-ground gas composition measurements (Table 1) [*Brandt et al.*, 2015]. The close correspondence of atmospheric enhancement ratios to the reservoir gas composition indicates that emissions to the atmosphere in the Bakken shale are dominated by loss of raw gas rather than processed gas.

Flux estimates were made using the mass balance technique for seven downwind flight legs on 4 days. These flights encompass wind from both the NW and S (Figure 2a). The use of multiple downwind legs with differing wind directions supports the calculation of a robust, representative flux for the campaign period while simultaneously illustrating that out-of-field sources are negligible. Key observed values for calculating mass balance fluxes are summarized in supporting information Table S1. Average ethane emissions of 27×10^3 kg/h were extrapolated to an annual emission of 0.23 ± 0.07 (2σ) Tg C_2H_6/yr. This extrapolation assumes constant emissions through the course of the year. We do not have observations at other times of year for the Bakken, but there is no reason to assume strong variance based on reported production [*U.S. Energy Information Administration*, 2016], and observations in other oil and gas basins have shown little seasonality [*Smith et al.*, 2015; *Karion et al.*, 2015; *Kort et al.*, 2014].

Uncertainty for each individual flight flux estimate was calculated and propagated following *Smith et al.* [2015], *Peischl et al.* [2015], and *Karion et al.* [2015], with values and results summarized in supporting information Table S1. Uncertainty for the mean flux is calculated from the variance in the individual downwind legs and reported in the manuscript as 2σ. We can also consider that the average single flight standard deviation from propagating uncertainty is ~40% (supporting information Table S1). If we calculate the standard error of the mean using 40% as the standard deviation, we find that twice the standard error calculated this way is 0.07—exhibiting consistency between the individual derived flight uncertainty and the variance observed over the course of the campaign.

4. Bakken Shale Contribution to Global Ethane Changes

Emissions of 0.23 Tg C_2H_6/yr represents 1–3% of total global ethane emissions from this single location. Annual ethane emissions are reported to have declined from 1986 to 2010 by 3.0 Tg in total [*Simpson et al.*, 2012]. Assuming a linear change in annual emissions, this corresponds to a decrease in emissions rate of 0.12 Tg/yr/yr. To estimate the annual change in emissions from the Bakken, we assume that emissions of ethane track production of natural gas in the basin (equivalent to assuming a constant leak rate with time). Figure 1 illustrates this emissions estimate from the Bakken as well as the rate of ethane emissions increase. This estimate indicates that the growth rate in emissions from the Bakken alone reached a sustained level in 2012 (0.06 Tg/yr/yr) sufficient to cancel half the average long-term decline rate in global ethane emissions. This is consistent with the hypothesis that the large increase in U.S. oil and gas production has led to a reversal in the declining atmospheric ethane burden and highlights the disproportionate role played by the Bakken region, which represented only 2% of shale gas production in the U.S. in May 2014 [*U.S. Energy Information Administration*, 2016] and yet emitted 1–3% of total global ethane emissions.

The very heavy composition of raw gas in the Bakken shale (42% molar C2:C1) helps explain the relatively high emissions. Other shale plays in the U.S. have notably lower ratios (Table 2). Considering other basins' relative production and raw gas composition, it is reasonable to suspect that emissions of ethane from the Eagle Ford combines with the Bakken to represent a large fraction of the recent global shift in ethane, whereas very dry formations such as the Haynesville and Fayetteville likely play a modest role in ethane emissions in spite of their large gas production. The Marcellus, a very productive formation, has been observed to have a low C2:C1 ratio [*Peischl et al.*, 2015], though some composition data suggest higher ratios [*Conder and Lawlor*, 2014; *Ghandi et al.*, 2015]. Observations in the Washington D. C. area in recent years have suggested increasing ethane emissions from the Marcellus [*Vinciguerra et al.*, 2015].

Table 2. Ethane:Methane (C_2:C_1) Molar Ratios of Major Shale Plays in the U.S. and Percentage of U.S. Shale Gas Production in May 2014[a]

Basin	Bakken	Eagle Ford	Marcellus	Barnett	Haynesville	Fayetteville	Utica
Molar % C2:C1	42[b]	25[c,f]	2[e] 16[c,f]	3[d] (dry) 15[d] (wet)	0.1[d]	1[d]	16[c,f]
% U.S. shale gas production	2	12	35	12	12	8	3

[a]Production from the *U.S. Energy Information Administration* [2016]; gas composition from well measurements reported in the following.
[b]*Brandt et al.* [2015].
[c]*Conder and Lawlor* [2014].
[d]*Speight* [2013].
[e]*Peischl et al.* [2015].
[f]*Ghandi et al.* [2015].

5. Implications for Tropospheric Ozone

Emissions of ethane, methane, and other VOCs from the Bakken have the potential to impact ozone formation on a variety of spatial scales. Local ozone enhancements observed during the Spring 2014 airborne study were relatively small due to low temperatures, large solar zenith angles, and generally high wind speeds. Initial Goddard Earth Observing System-Chem modeling (for details see supporting information Text S1) suggests that in summer, when surface ozone production peaks, up to 4 ppb of additional ozone are produced in plumes downwind of the Bakken region due to emissions of alkanes with composition as in Table 1 (Figure 3 and supporting information Movie S1). An increase of this magnitude could contribute to noncompliance with air quality regulations in affected areas downwind. More accurate modeling of the net impact of Bakken emissions on ozone formation would require additional measurement-based constraints on other reactive volatile organic compounds, including oxygenated compounds [*Edwards et al.*, 2015] and on nitrogen oxides [*Ahmadov et al.*, 2015] emitted from oil and gas activities in the region.

6. Conclusions

Much attention has focused on fugitive methane emissions from shale gas. This work demonstrates that we must also consider the impact of fugitive ethane emissions, particularly in basins where heavy gas composition leads to higher fugitive ethane efflux at similar volumetric leakage rates. The role of fugitive emissions with heavy gas composition also impacts assessments of global methane emissions from global ethane levels. Analyses that assume a temporally constant oil and gas production ethane:methane emission ratio

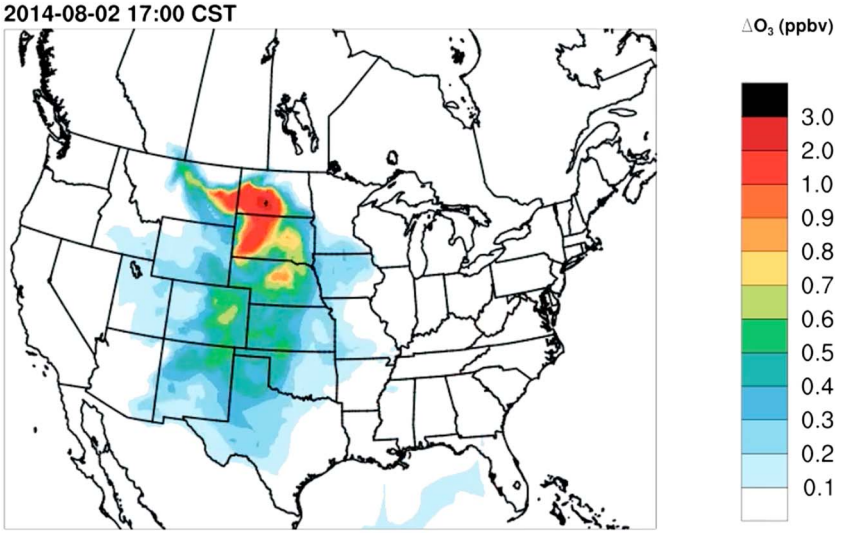

Figure 3. Simulation of change in surface ozone resulting from fugitive Bakken alkane (C2+) emissions, example for 2 August 2014 at 17:00 CST.

lower than present in the Bakken, or other productive basins, will erroneously conclude a large fossil methane emissions increase since 2010. Finally, the large, recently developed ethane source reported here has potential impacts on simulations of atmospheric composition in the last decade, as such a perturbation to ethane emissions are not presently represented in inventories and may impact representations of tropospheric ozone.

Acknowledgments
Data from the aircraft campaign reported in the manuscript are archived and available at http://www.esrl.noaa.gov/csd/groups/csd7/measurements/2014topdown/. This project was supported by the NOAA AC4 program under grant NA14OAR0110139 and NASA grant NNX14AI87G. J. Peischl and T. Ryerson were supported in part by the NOAA Climate Program Office and in part by the NOAA Atmospheric Chemistry, Carbon Cycle, and Climate Program. We thank Arlene Fiore (Columbia) for computational resources. We thank Anna Karion for assistance with fieldwork and manuscript comments, Michael Trainer for scientific direction and manuscript comments, and NOAA Aircraft Operations Center staff and flight crew for their efforts in helping collect these data.

References

Ahmadov, R., et al. (2015), Understanding high wintertime ozone pollution events in an oil- and natural gas-producing region of the western US, *Atmos. Chem. Phys.*, *15*, 411–429.

Aikin, A. C., J. R. Herman, E. J. Maier, and C. J. McQuillan (1982), Atmospheric chemistry of ethane and ethylene, *J. Geophys. Res.*, *87*, 3105–3118, doi:10.1029/JC087iC04p03105.

Barkley, M. P., et al. (2011), Can a "state of the art" chemistry transport model simulate Amazonian tropospheric chemistry?, *J. Geophys. Res.*, *116*, D16302, doi:10.1029/2011JD015893.

Blake, D. R., and F. S. Rowland (1986), Global atmospheric concentrations and source strengths of ethane, *Nature*, *321*, 231–233.

Brandt, A. R., et al. (2014), Methane leaks from North American natural gas systems, *Science*, *343*, 733–735.

Brandt, A. R., T. Yeskoo, S. McNally, K. Vafi, H. Cai, and M. Q. Wang (2015), Energy intensity and greenhouse gas emissions from crude oil production in the Bakken formation: Input data and analysis methods, Energy Syst. Div., Argonne Natl. Lab. [Available at https://greet.es.anl.gov/publication-bakken-oil.]

Caulton, D. R., et al. (2014), Toward a better understanding and quantification of methane emissions from shale gas development, *Proc. Natl. Acad. Sci. U. S. A.*, *111*, 6237–6242.

Collins, W. J., R. G. Derwent, C. E. Johnson, and D. S. Stevenson (2002), The oxidation of organic compounds in the troposphere and their global warming potentials, *Clim. Change*, *52*, 453–479.

Conder, M. W., and K. A. Lawlor (2014), Production characteristics of liquids-rich resource plays challenge facility design. [Available at http://www.aogr.com/magazine/editors-choice/production-characteristics-of-liquids-rich-resource-plays-challenge-facilit, retrieved August 17, 2015.]

Conley, S. A., I. C. Faloona, D. H. Lenschow, A. Karion, and C. Sweeney (2014), A low-cost system for measuring horizontal winds from single-engine aircraft, *J. Atmos. Oceanic Technol.*, *31*, 1312–1320.

Dlugokencky, E. J., R. C. Myers, P. M. Lang, K. A. Masarie, A. M. Crotwell, K. W. Thoning, B. D. Hall, J. W. Elkins, and L. P. Steele (2005), Conversion of NOAA atmospheric dry air CH_4 mole fractions to a gravimetrically prepared standard scale, *J. Geophys. Res.*, *110*, D18306, doi:10.1029/2005JD006035.

Draxler, R. R., and G. D. Rolph (2015), HYSPLIT (Hybrid Single Particle Lagrangian Integrated Trajectory) model, NOAA Air Resour. Lab., College Park, Md. [Available at http://www.arl.noaa.gov/HYSPLIT.php, access via NOAA ARL READY.]

Edwards, P. M., et al. (2015), High winter ozone pollution from carbonyl photolysis in an oil and gas basin, *Nature*, *514*, 351–354.

Etiope, G., and P. Ciccioli (2009), Earth's degassing: A missing ethane and propane source, *Science*, *323*, 478.

European Commission, Joint Research Centre JRC, and Netherlands Environmental Assessment Agency PBL (2011), Emission Database for Global Atmospheric Research (EDGAR), release version 4.2. [Available at http://edgar.jrc.ec.europa.eu.]

Fiore, A. M., J. T. Oberman, M. Y. Lin, L. Zhang, O. E. Clifton, D. J. Jacob, V. Naik, L. W. Horowitz, J. P. Pinto, and G. P. Milly (2014), Estimating North American background ozone in U.S. surface air with two independent global models: Variability, uncertainties, and recommendations, *Atmos. Environ.*, *96*, 284–300.

Franco, B., et al. (2015), Retrieval of ethane from ground-based FTIR solar spectra using improved spectroscopy: Recent burden increase above Jungfraujoch, *J. Quant. Spectros. Radiat. Transfer*, *160*, 36–49.

Ghandi, A., S. Yeh, A. R. Brandt, K. Vafi, H. Cai, M. Q. Wang, B. R. Scanlon, and R. C. Reedy (2015), Energy intensity and greenhouse gas emissions from crude oil production in the Eagle Ford Region: Input data and analysis methods, UC Davis Inst. of Transp. Stud., Prepared for Argonne Natl. Lab., Sept.

Giglio, L., J. T. Randerson, and G. R. van der Werf (2013), Analysis of daily, monthly, and annual burned area using the fourth-generation global fire emissions database (GFED4), *J. Geophys. Res. Biogeosci.*, *118*, 317–328, doi:10.1002/jgrg.20042.

Goldstein, A. H., S. C. Wofsy, and C. M. Spivakovsky (1995), Seasonal variations of nonmethane hydrocarbons in rural New England: Constraints on OH concentrations in northern midlatitudes, *J. Geophys. Res.*, *100*, 21,023–21,033, doi:10.1029/95JD02034.

Highwood, E. J., K. P. Shine, M. D. Hurley, and T. J. Wallington (1999), Estimation of direct radiative forcing due to non-methane hydrocarbons, *Atmos. Environ.*, *33*, 759–767.

Hudman, R. C., N. E. Moore, A. K. Mebust, R. V. Martin, A. R. Russell, L. C. Valin, and R. C. Cohen (2012), Steps towards a mechanistic model of global soil nitric oxide emissions: Implementation and space based-constraints, *Atmos. Chem. Phys.*, *12*, 7779–7795.

Karion, A., et al. (2013), Methane emissions estimate from airborne measurements over a western United States natural gas field, *Geophys. Res. Lett.*, *40*, 4393–4397, doi:10.1002/grl.50811.

Karion, A., et al. (2015), Aircraft-based estimate of total methane emissions from the Barnett shale region, *Environ. Sci. Technol.*, *49*, 8124–8131.

Keller, C. A., M. S. Long, R. M. Yantosca, A. M. Da Silva, S. Pawson, and D. J. Jacob (2014), HEMCO v1.0: A versatile, ESMF-compliant component for calculating emissions in atmospheric models, *Geosci. Model Dev.*, *7*, 1409–1417.

Kort, E. A., C. Frankenberg, K. R. Costigan, R. Lindenmaier, M. K. Dubey, and D. Wunch (2014), Four corners: The largest US methane anomaly viewed from space, *Geophys. Res. Lett.*, *41*, 6898–6903, doi:10.1002/2014GL061503.

Legendre, P., and L. Legendre (1998), *Numerical Ecology (Developments in Environmental Modeling)*, 2nd ed., Elsevier, Amsterdam.

Mao, J., F. Paulot, D. J. Jacob, R. C. Cohen, J. D. Crounse, P. O. Wennberg, C. A. Keller, R. C. Hudman, M. P. Barkley, and L. W. Horowitz (2013), Ozone and organic nitrates over the eastern United States: Sensitivity to isoprene chemistry, *J. Geophys. Res. Atmos.*, *118*, 11,256–11,268, doi:10.1002/jgrd.50817.

Murray, L. T., D. J. Jacob, J. A. Logan, R. C. Hudman, and W. J. Koshak (2012), Optimized regional and interannual variability of lightning in a global chemical transport model constrained by LIS/OTD satellite data, *J. Geophys. Res.*, *117*, D20307, doi:10.1029/2012JD017934.

North Dakota Drilling and Production Statistics (2015), Historical monthly gas production and sales statistics & historical monthly Bakken oil production statistics. [Available at https://www.dmr.nd.gov/oilgas/stats/statisticsvw.asp, accessed 9/16/15].

Peischl, J., et al. (2013), Quantifying sources of methane using light alkanes in the Los Angeles basin, California, *J. Geophys. Res. Atmos.*, *118*, 4974–4990, doi:10.1002/jgrd.50413.

Peischl, J., et al. (2015), Quantifying atmospheric methane emissions from the Haynesville, Fayettville, and northeastern Marcellus shale gas production regions, *J. Geophys. Res. Atmos.*, *120*, 2119–2139, doi:10.1002/2014JD022697.

Petron, G., et al. (2014), A new look at methane and nonmethane hydrocarbon emissions from oil and natural gas operations in the Colorado Denver-Julesburg Basin, *J. Geophys. Res. Atmos.*, *119*, 6836–6852, doi:10.1002/2013JD021272.

Rudolph, J. (1995), The tropospheric distribution and budget of ethane, *J. Geophys. Res.*, *100*, 11,369–11,381, doi:10.1029/95JD00693.

Schultz, M., et al. (2007), Emission data sets and methodologies for estimating emissions, *RETRO Proj. Rep. D1-6*, Hamburg, 26 Feb. [Avialable at http://retro.enes.org/reports/D1-6_final.pdf.]

Schwarz, J. P., J. S. Holloway, J. M. Katich, S. McKeen, E. A. Kort, M. L. Smith, T. B. Ryerson, C. Sweeneyand, and J. Peischl (2015), Black carbon emissions from the bakken oil and gas development region, *Environ. Sci. Technol. Lett.*, *2*(10), 281–285.

Simpson, I. J., M. P. Sulbaek Andersen, S. Meinardi, L. Bruhwiler, N. J. Blake, D. Helmig, F. Sherwood Rowland, and D. R. Blake (2012), Long-term decline of global atmospheric ethane concentrations and implications for methane, *Nature*, *488*, 490–494.

Smith, M. L., E. A. Kort, A. Karion, C. Sweeney, S. C. Herndonand, and T. I. Yacovitch (2015), Airborne ethane observations in the Barnett shale: Quantification of ethane flux and attribution of methane emissions, *Environ. Sci. Technol.*, *49*, 8158–8166.

Speight, J. G. (2013), *Shale Gas Properties and Processing*, 170 pp., Gulf Prof., Waltham, Mass.

U.S. Energy Information Administration (2016), Monthly dry shale gas production. [Available at http://www.eia.gov/naturalgas/weekly/, retrieved March 9, 2016.]

van Donkelaar, A., et al. (2008), Analysis of aircraft and satellite measurements from the Intercontinental Chemical Transport Experiment (INTEX-B) to quantify long-range transport of East Asian sulfur to Canada, *Atmos. Chem. Phys.*, *8*, 2999–3014.

Vinciguerra, T., S. Yao, J. Dadzie, A. Chittams, T. Deskins, S. Ehrman, and R. R. Dickerson (2015), Regional air quality impacts of hydraulic fracturing and shale natural gas activity: Evidence from ambient VOC observations, *Atmos. Environ.*, *110*, 144–150.

Wennberg, P. O., et al. (2012), On the sources of methane to the Los Angeles atmosphere, *Environ. Sci. Technol.*, *46*, 9282–9289.

Wild, O., X. Zhu, and M. J. Prather (2000), Fast-J: Accurate simulation of in- and below-cloud photolysis in tropospheric chemical models, *J. Atmos. Chem.*, *37*, 245–282.

Xiao, Y., J. A. Logan, D. J. Jacob, R. C. Hudman, R. Yantosca, and D. R. Blake (2008), Global budget of ethane and regional constraints on U.S. sources, *J. Geophys. Res.*, *113*, D21306, doi:10.1029/2007JD009415.

Yacovitch, T. I., et al. (2014), Demonstration of an ethane spectrometer for methane source identification, *Environ. Sci. Technol.*, *48*, 8028–8034.

Zhang, L., D. J. Jacob, X. Yue, N. V. Downey, D. A. Wood, and D. Blewitt (2014), Sources contributing to background surface ozone in the US Intermountain West, *Atmos. Chem. Phys.*, *14*, 5295–5309.

Letter

Reversal of global atmospheric ethane and propane trends largely due to US oil and natural gas production

Detlev Helmig , Samuel Rossabi, Jacques Hueber, Pieter Tans, Stephen A. Montzka, Ken Masarie, Kirk Thoning, Christian Plass-Duelmer, Anja Claude, Lucy J. Carpenter, Alastair C. Lewis, Shalini Punjabi, Stefan Reimann, Martin K. Vollmer, Rainer Steinbrecher, James W. Hannigan, Louisa K. Emmons, Emmanuel Mahieu, Bruno Franco, Dan Smale & Andrea Pozzer

Nature Geoscience **9**, 490–495 (2016)
doi:10.1038/ngeo2721
Download Citation

Atmospheric chemistry Databases

Received: 12 November 2015
Accepted: 22 April 2016
Published online: 13 June 2016

Abstract

Non-methane hydrocarbons such as ethane are important precursors to tropospheric ozone and aerosols. Using data from a global surface network and atmospheric column observations we show that the steady decline in the ethane mole fraction that began in the 1970s[1,2,3] halted between 2005 and 2010 in most of the Northern Hemisphere and has since reversed. We calculate a yearly increase in ethane emissions in the Northern Hemisphere of 0.42 (±0.19) Tg yr^{-1} between mid-2009 and mid-2014. The largest increases in ethane and the shorter-lived propane are seen over the central and eastern USA, with a spatial distribution that suggests North American oil and natural gas development as the primary source of increasing emissions. By including other co-emitted oil and natural gas non-methane hydrocarbons, we estimate a Northern Hemisphere total non-methane hydrocarbon yearly emission increase of 1.2 (±0.8) Tg yr^{-1}. Atmospheric chemical

transport modelling suggests that these emissions could augment summertime mean surface ozone by several nanomoles per mole near oil and natural gas production regions. Methane/ethane oil and natural gas emission ratios could suggest a significant increase in associated methane emissions; however, this increase is inconsistent with observed leak rates in production regions and changes in methane's global isotopic ratio.

Main

Oxidation of atmospheric non-methane hydrocarbons (NMHCs) contributes to production of surface ozone and secondary aerosol, both of which impact air quality and climate. NMHCs are emitted into the atmosphere from a variety of biogenic and anthropogenic sources. Ethane is the longest-lived and most abundant NMHC, found typically at ~0.4–2.5 nmol mol^{-1} (ppb) in the background atmosphere. It is released from seepage of fossil carbon deposits, volcanoes, fires, and from human activities, with fossil fuel extraction, distribution leakage, and industrial use being the main sources. Pre-industrial ethane atmospheric mole fractions measured in polar ice cores were ~400 pmol mol^{-1} in the Northern Hemisphere (NH) and ~100 pmol mol^{-1} in the Southern Hemisphere (SH), that is between ~1/4–1/2 of current levels[4]. Firn air records[1,2,3] show that in the early part of the twentieth century NMHCs increased steadily in the global atmosphere. Light alkane NMHCs (C_2–C_5) reached a maximum that was ~50% above 1950 levels during 1970–1985. Global atmospheric ethane peaked around 1970. NMHCs have since been steadily declining to mole fractions that are closer to the earliest data in the Greenland firn record (Fig. 1a). These trends are primarily due to stricter air quality emission controls that were first implemented some 50 years ago with the goal to reduce human exposure to NMHCs and surface ozone. The regulations resulted in reduced emissions from sources such as the oil and natural gas (O&NG) industries and automobiles, and a gradual decline of atmospheric NMHCs in urban air in many developed countries and also in the background atmosphere[5,6,7].

Figure 1: Histories of atmospheric ethane.

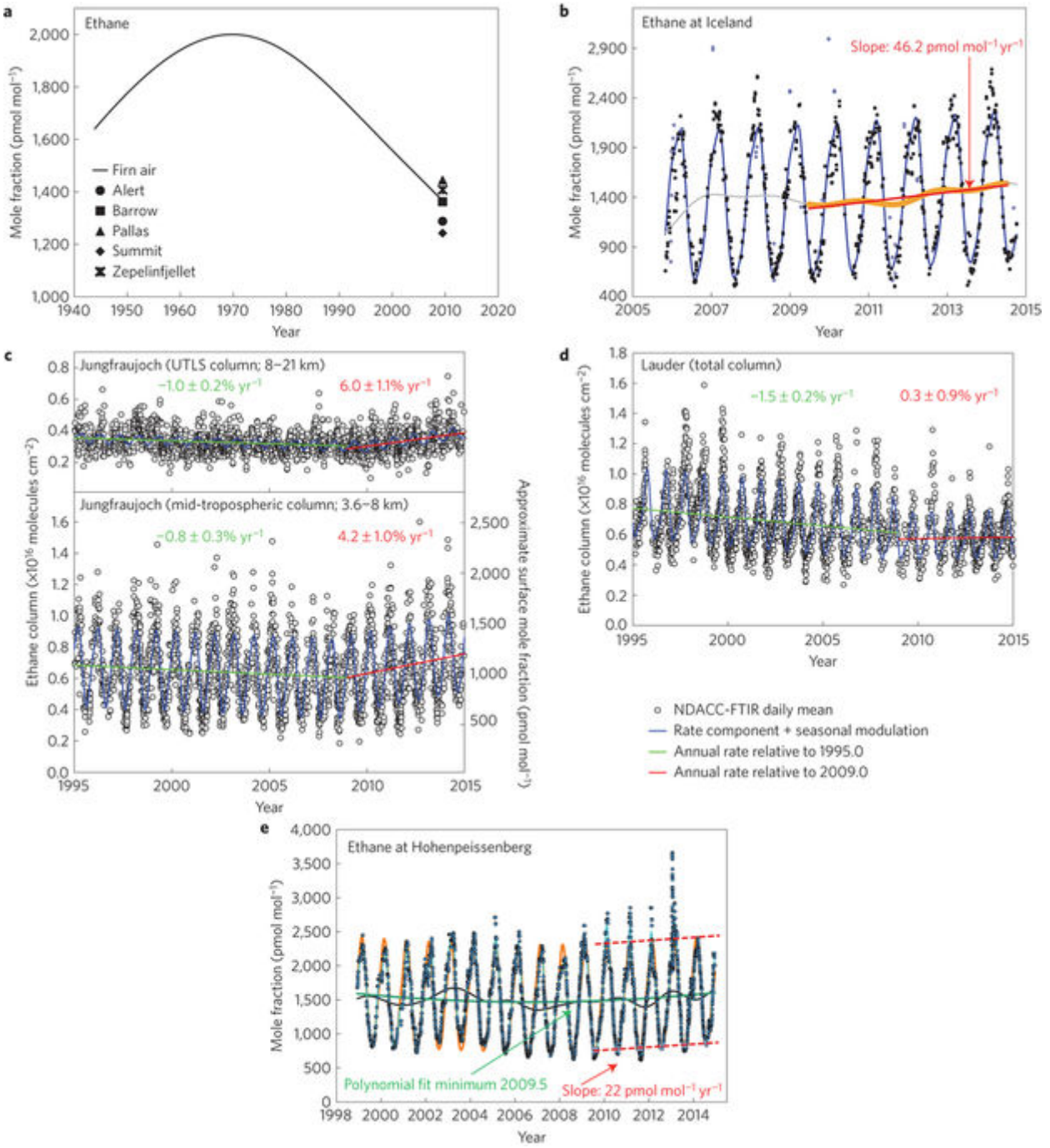

a, Reconstructed 1950–2010 ethane history from firn air sampling at NEEM in Greenland[3] with 2009.5 mean seasonally detrended atmospheric values at five Arctic sites for comparison. Data from ref. 3. **b**, Ten years of NMHC flask network data in south Iceland. Individual flask data, identified outliers (smaller blue points), a smoothed fit, the trend results after removal of harmonic components, and the linear regression fit are shown, with a 46.2 pmol mol^{-1} yr^{-1} increase from 2009.5 to 2014.5. **c**,**d**, Ethane upper troposphere and lower stratosphere (UTLS), and mid troposphere FTIR columns showing a trend reversal and increasing rate of change after 2009 at Jungfraujoch, Switzerland (**c**), in contrast to Lauder, New Zealand (**d**). **e**, Monthly running median data from the daily *in situ* record at Hohenpeissenberg, with smoothed, function, and trend fits. A polynomial fit shows a minimum in the second half

of 2009; the linear regression to the post 2009.5 trend curves and seasonal maxima and minima show increases of 22–23 pmol mol^{-1} yr^{-1}.

Ethane and methane are co-emitted from O&NG sources. Ethane observations have been used to attribute anthropogenic methane emission changes[7]. Having the longest NMHC lifetime, of the order of 2 (summer) to 6 (winter) months, ethane is the NMHC observed with the least spatial and short-term variability in background air, making it the best candidate species for studying hemispheric gradients and long-term changes.

We analysed ten years of NMHC data collected at 44 remote global sampling sites from the National Oceanic and Atmospheric Administration (NOAA) Global Greenhouse Gas Reference Network (GGGRN). We also include data from *in situ* monitoring at Summit, Greenland[8], at Hohenpeissenberg (HPB) in Southern Germany[9], Jungfraujoch (JFJ) and Rigi, Switzerland, and Cape Verde in the Mid-Atlantic[10]. For propane, we further included results from eight sites within NOAA's GGGRN (Methods).

Atmospheric NMHCs exhibit a dynamic seasonal and latitudinal behaviour. Maxima are seen in late winter, and minima in the summer (Fig. 1b–e). Sources of light NMHCs do not vary much seasonally[11]; seasonal cycles are primarily driven by photochemical loss. Consequently, seasonal cycles exhibit the largest amplitude near the poles, are small near the Equator (Fig. 2), and are shifted by ~6 months in the SH owing to the opposite season. There is also a strong latitudinal gradient of absolute values, with highest abundances observed in the Arctic, steeply declining levels at mid-latitudes, and lower abundance in the SH. These gradients are caused by sources that are dominated by anthropogenic emissions, which are highest in the industrialized mid-northern latitudes, and the slower transport across the equatorial zone compared with intrahemisphere mixing. Gases with shorter lifetimes, that is, propane, *i*so-butane, and *n*-butane, exhibit more pronounced seasonal and latitudinal gradients (Fig. 2).

Figure 2: Latitudinal distribution of ethane, propane, *iso*-butane, and *n*-butane.

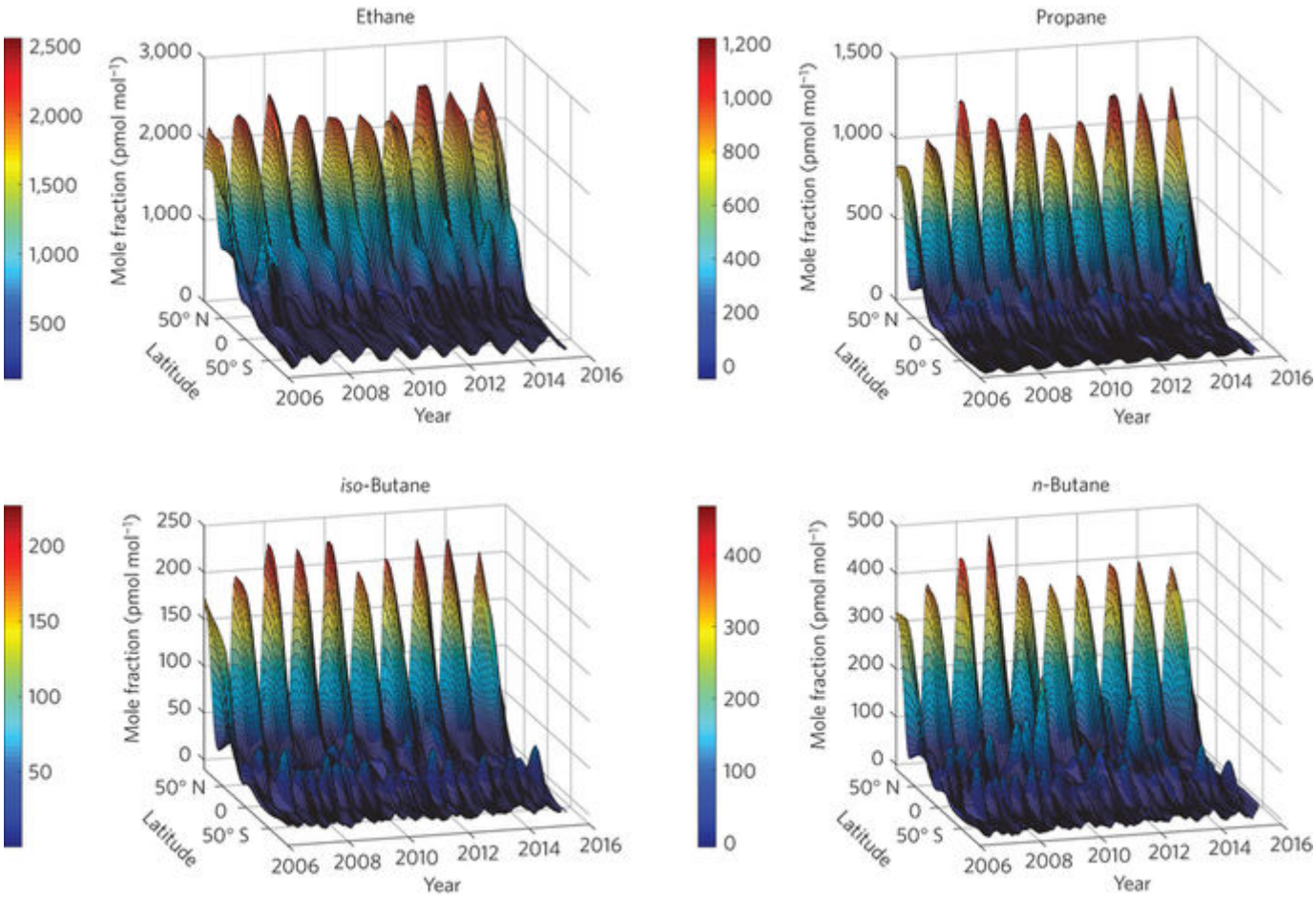

These representations of surface mole fractions were generated using weekly data from 37 to 39 global background monitoring sites, altogether some 30,000 data points for each graph. Note that these plots are a representation of latitudinal averages of atmospheric mole fractions; therefore, they do not capture differences between continents at the same latitude. Procedures for data filtering and processing are discussed in the Methods.

Individual site data reveal that for many NH locations the downward trend reported in earlier work has halted and reversed to increasing NMHC levels. As the flask network programme started in 2006, data for most sites do not go back far enough for deciphering the exact time of the trend reversal. The second-order polynomial fit through the longest, and most highly time-resolved *in situ* record from HPB has its minimum in 2009 (Fig. 1e), in agreement with the JFJ Fourier transform infrared (FTIR) column observations (Fig. 1c). Focusing on the most recent five years (2009.5–2014.5) we find variable results in the observed rate of change; however, a consistent picture emerges that shows the largest increases at NH sites (Fig. 3). Of 32 NH sites, 9 exhibit

ethane growth rates >50 pmol $mol^{-1}yr^{-1}$, and 13 sites exhibit growth rates between 25 and 50 $pmol^{-1}$ $mol^{-1}yr^{-1}$ (Supplementary Table 1). Depending on grouping of sites and averaging across regions and calculation method, a mean NH ethane increase rate of 2.9–4.7% yr^{-1} is calculated (Methods). These rates of change in atmospheric ethane have not been seen at SH sites; most SH sites show only small changes, with poorer regression results. Applying a second-order polynomial fit to the NH trend curves yields positive quadratic coefficients in 22 out of 32 cases, showing that for most cases, ethane trend curves are becoming steeper; that is, rates of change in atmospheric abundance have been increasing at most of the sites during this time window.

Figure 3: Ethane and propane trends at global monitoring sites.

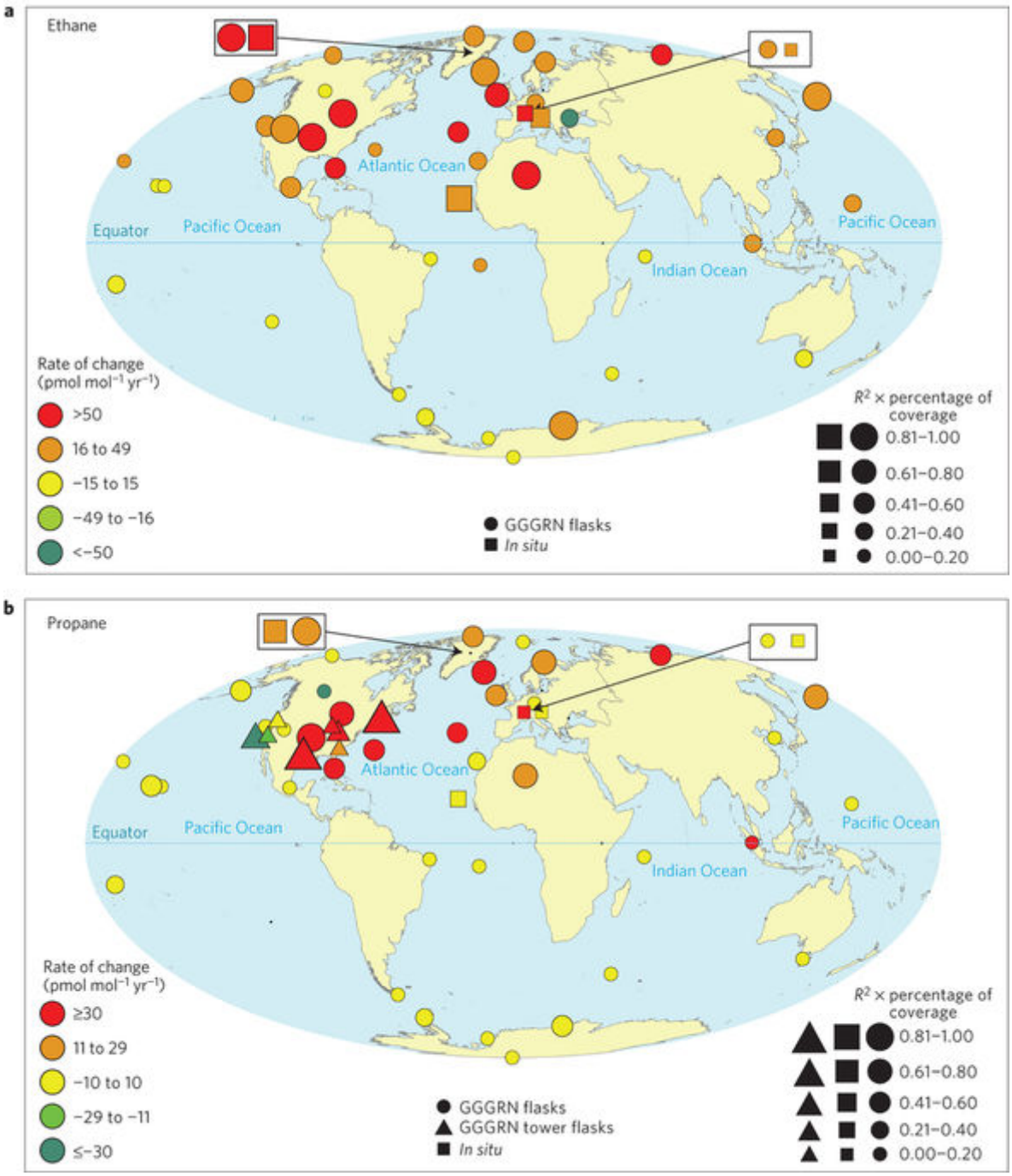

Mole fraction changes are indicated by the colour scale with marker size corresponding to the R^2 of the fit multiplied by the fraction of available site data. Results from overlapping GGGRN flask and *in situ* measurements are shown in black rectangles for Summit and Hohenpeissenberg. **a**, Increasing ethane is observed throughout the NH, with the strongest signal in North America, the North Atlantic, and neighbouring continents. There is no or very little change in ethane at SH sites. **b**, Propane shows a more pronounced region of increasing mole fractions in the eastern USA and at nearby downwind sites. Again, these changes are not seen at the SH sites.

This hemispheric difference in ethane trends is further supported by two contrasting records of ethane column observations (that is, the number of molecules integrated between the ground and the top of the atmosphere), one from JFJ (Fig. 1c)[12], and the other one from Lauder, New Zealand (Fig. 1d). At the 3,580 m elevation of JFJ, these data are a good representation of free tropospheric ethane, reflecting the continental background and long range transport. Whereas there was a slight downward trend in the data for the first 15 years of the record, in agreement with the trends inferred from the firn and HPB data, a reversal is evident after 2009, with a post-2009 rate of increase in the mid-troposphere of 4.2 ± 1.0% yr^{-1}. The upward trend is evident in both the mid-troposphere and upper troposphere/lower stratosphere partial columns, indicative of the hemispheric nature of the ethane increase. The ethane trend reversal is absent in the SH FTIR column data (Fig. 1d). The difference in trends in the hemispheres is consistent with an increasing NH source.

Notably, ethane rates of change are highest at the central and eastern USA and nearby downwind sites, suggesting that the ethane increase is driven to a large part by emissions from North America. The regional hotspot of increasing NMHC levels can be pinpointed more narrowly from propane observations. Propane, with a lifetime ~1/4 of ethane, is a more sensitive indicator for local/regional emissions. Propane data show the greatest increases in the central and eastern USA, and in the downwind North Atlantic region (Fig. 3). In contrast, propane levels have been relatively stable in central Europe, the Pacific region, and the SH. Also, measurements in the western USA do not show propane increases. With the primary synoptic transport direction being west and southwest to east, the spatial analyses of ethane and propane increases point to the central to eastern parts of the USA as the regions where most of the emission increases have occurred.

The O&NG sector is a major source of light NMHC emissions. A surge in O&NG production has occurred in recent years, particularly in the USA, where unconventional oil and natural gas drilling has resulted in estimated 10–20-fold increases in shale O&NG production between 2000 and 2015 (www.eia.gov), making the USA the fastest growing and a leading O&NG producing nation. Ground and airborne observations have consistently shown elevated levels of methane and NMHC as a result of venting, flaring, and leakage. NMHC ambient mole fractions measured in O&NG basins can far exceed (up

to >100 times) the regional background and those in urban and other industrial regions, and top-down emission estimates are well above inventory estimates[13,14,15,16,17]. Resulting ozone production from these emissions has led to air quality standard exceedances in the Uintah Basin, Utah, and Upper Green River Basin, Wyoming, O&NG regions[18,19]. Two other regional studies have previously noted upwards trends in ambient NMHC and associated these changes with upwind O&NG activities. An increase from 7% to 13% of the total observed non-methane organic carbon abundance during 2010–2013, and increasing ethane mole fractions were measured in Baltimore, Maryland, downwind of the Marcellus Shale[20]. Similarly, data from southern Texas showed steeply increasing ethane levels associated with transport from the Eagle Ford Shale[21].

Applying the JFJ FTIR mid-troposphere column trend value of 4.2% yr^{-1} to the NH annual ethane emission estimate of 9.9 Tg yr^{-1} (Methods) yields an estimate for an ethane annual emission increase of 0.42 ± 0.19 Tg yr^{-1} (see Methods for all uncertainty range calculations), resulting in an overall 2.1 ± 1.0 Tg yr^{-1} emission increase during 2009.5–2014.5. This additional emission is ~1.5 times the North America inventory estimate of 1.6 Tg yr^{-1} for 2007. Considering estimates of co-emitted NMHC yields an estimate for a yearly total NMHC emissions increase of 1.2 ± 0.8 Tg yr^{-1} (5.9 ± 4.0 Tg yr^{-1} overall emissions increase during 2009.5–2014.5).

There is no evidence for major non-O&NG NMHC emissions increases. From the spatial overlap of USA O&NG regions with identified areas of largest NMHC increases it seems likely that the NMHC increase is largely driven by USA O&NG production. This added NMHC emission is expected to fuel additional surface ozone production in source and downwind regions. Figure 4 illustrates modelling results from a first order of magnitude sensitivity study, where the 4.2% yr^{-1} increase in the C_2–C_5 NMHC flux was attributed to USA O&NG emissions over five years at constant emissions of nitrogen oxides (NO_x). This added emission causes changes in surface ozone in regions with O&NG development and downwind, reaching up to 0.5 nmol mol^{-1} yr^{-1} average ozone increases for June–August, corresponding to 2.5 nmol mol^{-1} increases overall over the five year period simulated with the model. The sensitivity is particularly high in the western USA, mostly driven by higher NO_x in that region. Consequently, these NMHC emission changes can potentially

offset emission controls that have been implemented for curbing photochemical ozone production, and therefore can be a concern for attaining the ozone air quality standard.

Figure 4: Ozone sensitivity study.

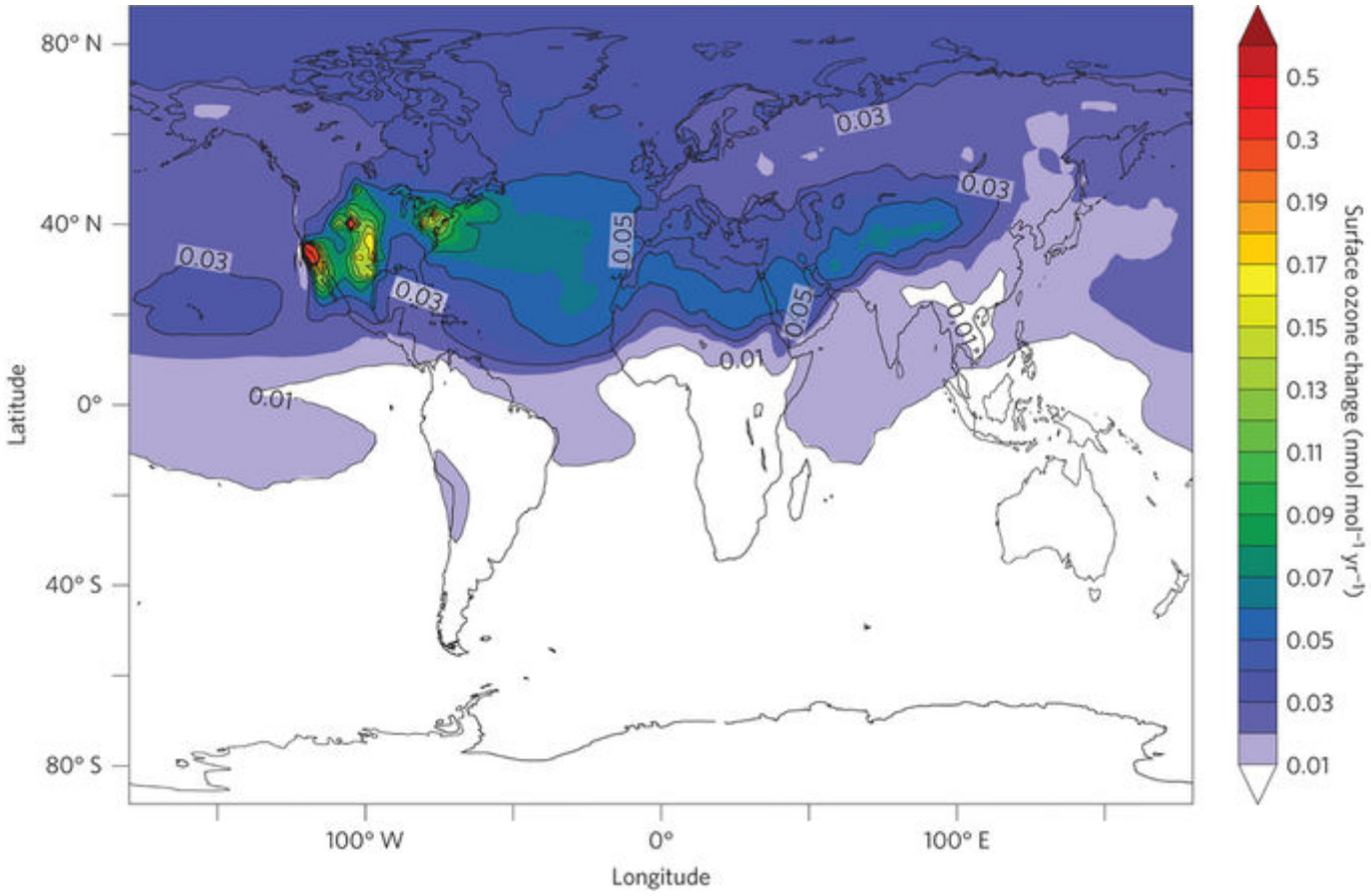

Estimate for the average annual 2009.5–2014.5 June–August change in surface ozone from a 4.2% yr^{-1} NH increase in ethane, and inferred emission increases in propane, butane and pentane isomers from USA O&NG sources. The modelling did not consider increases in methane and NMHC > C_5 emissions, and assumed constant emissions of nitrogen oxides and volatile organic compounds from other emission sectors. Increases in surface ozone are predicted over extended areas of the USA and downwind.

Atmospheric methane has been increasing since ~2007, after a ~8 year period of stable levels. Continental emission changes in methane are difficult to decipher because of the variety of biological, burning, and O&NG-related emissions, and the fact that trends are small relative changes in the large methane background. With shorter atmospheric lifetimes, trends of NMHC are more noticeable on a regional scale. Methane and ethane are co-emitted from O&NG sources in mass ratios of 1.7–33, with most results ranging

from 7 to 14 (Supplementary Table 5). If we assume that the added ethane emission is entirely from O&NG sources, that the methane/ethane ratio from O&NG has not changed over time, and considering a median source region methane/ethane emission ratio of 10, an increase in the anthropogenic methane emission of 4.4 ± 3.1 Tg yr^{-1} is estimated for the NH each year during 2009.5–2014.5. The cumulative increase in methane emissions implied from this approach would represent more than a doubling of O&NG-related methane USA inventory emissions[22] and a ~6.2% total increase between 2009.5 and 2014.5 of the 330 Tg yr^{-1} (ref. 23) global anthropogenic methane emission. Although other recent studies[12,24,25,26] have derived similar estimates for methane emission increases and associated those with increased North American O&NG emissions, most also rely on the extrapolation of NMHC results to infer methane emission changes. We note that surface and aircraft observations of methane stable isotopes from the GGGRN are inconsistent with such a large North American methane flux increase from O&NG sources[27]. Furthermore, the methane emission implied by this analysis of NMHC data as a fraction of O&NG production is a substantially higher percentage than what has been observed in O&NG fields in North America[13,17,28,29,30]. This suggests yet unidentified increasing sources for NMHC emissions independent of methane or with lower methane/ethane emission ratios, or potential emission increases outside North America that cannot be well defined at present owing to the sparsity of observations in those regions (for instance, in the Middle East, Africa, and Asia).

Methods

Global VOC network.

Since 2004 the NOAA GMD and INSTAAR in Boulder, Colorado, have been operating a global volatile organic compound (VOC) monitoring programme that is building on the NOAA Global Greenhouse Gas Reference Network (GGGRN). VOCs are quantified in whole air sampled in pairs of glass flasks that are collected weekly to bi-weekly at ~44 global background monitoring sites, with a total sample number of ~3,000 per year. At present, ethane, acetylene, propane, *i*so-butane, *n*-butane, iso-pentane, *n*-pentane, isoprene, benzene, and toluene are analysed in the sample remaining in the flasks after completion of analyses of greenhouse gases, and of CO_2 and methane stable isotopic

ratios. The gas chromatography (GC) with flame ionization detection method[31] is calibrated by a series of gravimetrically prepared synthetic and whole air standards. The programme operates under the umbrella of the World Meteorological Organization Global Atmospheric Watch (WMO-GAW) and is collaborating with international partners on exchange of calibration standards and comparison of calibration scales[32]. The INSTAAR laboratory was audited by the World Calibration Center (WCC) for VOC[33] in 2008 and 2011. Five unknown standards were analysed and results reported to the WCC. Mean results of five repeated measurements of the provided standards deviated <1.5% ethane, and <0.8% for propane from the certified values. These deviations are well below the deviation criteria set by GAW[34]. Uncertainties in the NMHC data are estimated to be ≤5% for results >100 pmol mol^{-1}, and ≤5 pmol mol^{-1} for results <100 pmol mol^{-1}. More analytical and programme details are provided by refs 31,35,36.

VOC *in situ* monitoring at Summit (SUM), Greenland.

Year-round VOC monitoring at Summit (72.6 °N, 38.5 °W; 3,216 m asl) was performed from 26 June 2008 to 22 July 2010, totalling 756 days (just over 2 years)[37], and resumed in May 2012 and is ongoing. The GC is calibrated several times per week using standards that are cross-referenced against the global flask network laboratory scale. Uncertainties in the NMHC data are estimated to be ≤5% for results >100 pmol mol^{-1}, and ≤5 pmol mol^{-1} for results <100 pmol mol^{-1}.

VOC *in situ* monitoring at Hohenpeissenberg (HPB).

Continuous VOC monitoring at HPB (47.8 °N, 11.8 °E, 980 m asl) has been conducted since 1998 as part of the WMO-GAW[9]. Calibrations rely on a series of gravimetric and whole air standards referenced to the WCC. VOC sampling is conducted daily at noontime. Uncertainties (95% confidence interval) are generally ± (1.9 pmol mol^{-1} + 2.9%) in the ethane mole fraction, and ± (1.3 pmol mol^{-1} + 2.9%) for propane, except for isolated periods of degraded chromatography or other instrumental issues that result in higher uncertainties. Detection limits are at ~3 and 2 pmol mol^{-1} for ethane and propane, respectively.

VOC *in situ* monitoring at Jungfraujoch (JFJ).

At JFJ, a high-elevation site in the central Swiss Alps (46.5 °N, 7.6 °E, 3,580 m asl), VOCs are measured using a Medusa GC/mass spectrometer (MS)[38] hourly with each pair of measurements bracketed by standard measurements. Ethane and propane measurements started in 2008 and are ongoing. Measurement precisions are 0.3% for ethane and 0.8% for propane (1σ). Calibration is provided by referencing standards against primary reference gases of the National Physical Laboratories (UK) and thus is linked to the WMO-VOC scale. Uncertainties are ~10% for ethane and 3% for propane.

VOC *in situ* monitoring at Cape Verde (CVO).

The Cape Verde Atmospheric Observatory Humberto Duarte Fonseca (16.8 °N, 24.9 °W, 10 m asl) is positioned upwind of Calhau on the northeastern side of São Vicente, Cape Verdes. Hourly VOC measurements are made from a height of 20 m asl; analytical details are provided by ref. 10. Uncertainties in the NMHC data are estimated to be ≤5% for results >100 pmol mol^{-1}, and ≤5 pmol mol^{-1} for results <100 pmol mol^{-1}. Detection limits are 2.6 and 1.6 pmol mol^{-1} for ethane and propane, respectively. Calibrations are linked to the WMO-VOC scale.

VOC measurements from North American tower sites.

Glass flasks are also collected with automated samplers at tower sites across North America as part of the NOAA GGGRN. These samples are collected at a higher sampling frequency (~daily) and are analysed at NOAA by GC/MS[13]. Reported mole fractions for propane are based on a suite of gravimetric standards prepared at NOAA; calibration consistency is maintained independently from INSTAAR. The resulting NOAA calibration scale for propane has been assessed in an international round-robin exercise and was found to be consistent within 5% to other internationally recognized and well-established scales[39].

Data processing.

At the time of the data processing final data from all considered sites until June 2014 (2014.5) were available, which was used as the cutoff of the analyses. The criterion for individual sites data to be included was that data were available for at least 50% of the sampling days for 2009.5–2014.5. Two flask network and three tower site data sets were excluded because they did not meet this criterion. Similarly, *in situ* data from remote

monitoring sites were only included if data were available for at least 50% of the 2009.5–2014.5 sampling dates.

NMHC data were first filtered for outliers; values that deviated more than 2σ from a running median were excluded from trend analyses. Filtered data were then uploaded to the NOAA server for filtering and trend determination using the method of ref. 40 and described at http://www.esrl.noaa.gov/gmd/ccgg/mbl/crvfit/crvfit.html. The first step is to fit a function, consisting of the sum of a polynomial and four harmonics (amplitude and phase of 1 through 4 cycles per year). The residuals of the function fit are smoothed by two low-pass filters, one for the trend (1.1 year full-width at half-maximum), and one for anomalies of the seasonal cycle (full-width at half-maximum 50 days). The function and filtered data are then combined to generate a smoothed data curve, trend curve, a detrended seasonal cycle, seasonal amplitude, a polynomial fit, and the long-term growth rate. The smoothed data curve is a combination of the function and the short-term filter of the residuals. The trend curve is the polynomial part of the function plus the long-term filtered residuals, and represents the growth or decline of the data with the seasonal oscillations removed. The detrended seasonal cycle is complementary to the trend curve; it is the interannually varying cycle with the trend removed. The seasonal amplitude is the amplitude of the detrended seasonal cycle, and the growth rate is the rate of increase or decrease of the trend, found by taking the first derivative of the trend. Results of a trends statistical significance test are included in Supplementary Tables 1 and 2. To avoid a bias from oversampling of the trend curve, its output was sampled only at times when retained flask data were available. These data were then subjected to the Mann–Kendall test[41] using a significance value of $\alpha = 0.01$. Results (calculated p values) are presented in column 12 of Supplementary Tables 1 and 2. Values <0.01 reflect the rejection of the null-hypothesis that there is no trend. In these cases, the trend is found to be true at 99% confidence. Incidences where trends were found to be not statistically significant are listed in italic font and in brackets. Results show that of 34 NH ethane trend series (flask and *in situ*), 32 show a positive trend. All positive trends are statistically significant. Lac La Biche, Alberta (LLB), shows a slight, nonsignificant negative trend. The LLB series has a reduced data coverage (73%), a high number of outlier points, and an $R^2 = 0$ result, all of which reduce the robustness of the LLB trend result. The other site showing a negative trend is Black Sea, Constanta (BSC). Similar to

LLB, this site suffers from reduced data coverage (50%), and a high number of outlier points. Furthermore, this site seems to be severely impacted by nearby pollution sources. Despite these two sites showing rather noisy records and poor regression results, they were retained in the presentation of our results, as we did not want to use arbitrary filtering criteria.

The data used in the maps (Fig. 3) were generated by applying a linear least-squares fit of the trend data from each site for the period 2009.5–2014.5. The slope of the fit determined the colour of the marker. The R^2 value times the coverage of the fit determined the size of the marker. Most of the data are from NOAA/INSTAAR network flask sites. Furthermore, *in situ* monitored sites were included, as well as propane data from the tower sites.

Easter Island (EIC) propane data were excluded because they showed influence from a local source. Propane network data from BSC, and propane tower flask data from Mount Wilson Observatory (MWO) were excluded because a representative fit could not be drawn. A summary of trend results from all surface network and tower flask, and *in situ* observations is provided in Supplementary Table 1 for ethane, and in Supplementary Table 2 for propane.

Network flask–*in situ* trend results evaluation.

There is overlap of flask and *in situ* VOC monitoring at two sites, that is, SUM and HPB. The parallel observations at these two sites were used to evaluate the quality of the trend fit results from the weekly network flask measurements against the higher time resolution *in-situ* measurements. Details of these comparison studies will be presented in a forthcoming publication. In summary, these investigations showed that the less frequent flask records provide a good representation of the *in situ* records, yielding trend results of the same magnitude (Fig. 3).

Average ethane trend calculations.

There are 45 sites that met the requirements (>50% data coverage for 2009.5–2014.5) for inclusion in the trend analyses, with 32 of these sites in the NH. As can be seen in Supplementary Tables 1 and 2, data coverage, quality of the correlation analyses, and

trend results vary widely. We explored a number of methods for deriving an average NH ethane trend from these data. First, data from all sites, regardless of data coverage and quality of the regression fit, were treated equal. For sites with flask and *in situ* data, the mean of both trend values was used (SUM and HPB). Sites were grouped by latitude zone, NH longitude, and continental/oceanic region, and average and median ethane trends were calculated from all sites within each region (Supplementary Table 3). Please note the uneven representation of regions, as some of them have fewer sites than others, making results for regions with low representation less certain. Depending on the grouping and averaging, ethane trend results range from 3.5 to 4.3% yr^{-1} for the mean values, and 2.9–4.2% yr^{-1} for the median results across all sub-regions. The lower mean values are largely due to the negative trend (–7.6% yr^{-1}) at BSC, a site that suffers from reduced data coverage (50%), and a high number of outliers, and seems to be severely impacted by nearby pollution sources (see above). Nonetheless, we kept the BSC result in the calculations for treating all sites equally for the NH mean trend calculations. Rates of increases are relatively high at Tiksi (TIK). Monitoring at TIK began in autumn 2011; therefore, the Tiksi record misses the first two years of the 2009.5–2014.5 window. The data coverage is just slightly above the 50% cutoff value (Supplementary Tables 1 and 2). TIK is the site with the second lowest coverage of all sites that were included. Given the short record the uncertainty is much higher than for other sites.

Second, a mean NH ethane trend was calculated by weighting each individual trend result (Supplementary Table 1) by the percentage of coverage of the data, and the R^2 of the linear regression fit. For the two sites with flask and *in situ* measurements the mean value of both trends, a 100% coverage value, and the sum of both R^2 values was used, to reflect the higher certainty from having two parallel results. The result of this analysis was a NH ethane increase rate of 4.7% yr^{-1}. This value is relatively strongly influenced by the two highest individual results from two sites in the central USA, that is, Southern Great Plains (SGP) with a rate of change of 10.7% yr^{-1}, and Park Falls (LEF), Wisconsin, with a value of 7.9% yr^{-1}, also because both sites have full data coverage, and relatively high R^2 results. Removing these two sites reduces the mean NH ethane rate of change to 4.2% yr^{-1}. It is notable, though, that sites that are far distant from local influences, by horizontal separation, elevation, or by both, and located in the Atlantic region, downwind of North America, showed the cleanest records, that is, the highest correlation

coefficient and on average relatively high rate of change values. Sites that fall into these categories (with their rate of change and R^2 results) are SUM (63.9 pmol mol^{-1} yr^{-1}, 4.7% yr^{-1}, R^2 = 0.97 for flask results and 67.2 pmol mol^{-1} yr^{-1}, 5.4% yr^{-1}, R^2 = 0.96 for *in situ*), Iceland (ICE) (46.2 pmol $mol^{-1}yr^{-1}$, 3.4% yr^{-1}, R^2 = 0.86), Mace Head (MHD) (53.1 pmol mol^{-1} yr^{-1}, 4.3% yr^{-1}, R^2 = 0.65), Azores (AZR) (86.7 pmol mol^{-1} yr^{-1}, 7.7% yr^{-1}, R^2 = 0.57), Assekrem (ASK) (72.9 pmol mol^{-1} yr^{-1}, 7.4% yr^{-1}, R^2 = 0.95), Tenerife (IZO) (30.0 pmol mol^{-1} yr^{-1}, 3.5% yr^{-1}, R^2 = 0.32) and CVO (44.7 pmol mol^{-1} yr^{-1}, 5.6% yr^{-1}, R^2 = 0.96). The mean weighted ethane rate of change from these North Atlantic sites accounts to 5.3% yr^{-1}. These comparisons point towards highest rates of ethane increase in the central to eastern USA, followed by the North Atlantic region.

The overall hemispheric ethane trend result of 4.7% yr^{-1} from the latter method using R^2 × coverage as a weighting factor is 0.4–1.8% yr^{-1} higher than the regional results presented in Supplementary Table 3. This possibly reflects a bias in the calculation as it places lower weight on sites with flat trends and corresponding low R^2 results.

The uncertainty (0.9%) of the best estimate of the ethane NH rate of change was determined as 1/2 of the range of the lowest (2.9%) to the highest value (4.7%) of the different types of regional and hemispheric trend determination.

NMHC surfaces.

Graphs in Fig. 2 were derived using weekly data from the GGGRN sites. To reduce noise in the latitudinal distribution due to synoptic-scale atmospheric variability, records were fitted with a smooth curve[40]. We then used a data extension methodology[42] with important revisions[43] to produce a set of smoothed records, which are synchronized in time and have no temporal gaps. For each synchronized weekly time step, a latitude distribution (mole fraction versus sine of latitude) was constructed. Each value in the weekly distribution was assigned a relative weight using a strategy that assigns greater significance to sites with high signal-to-noise and consistent sampling. A curve was then fitted to each weekly weighted latitudinal distribution[44]. Finally, values were extracted from each weekly latitudinal fit at intervals of 0.05 sine of latitude from 90 °S to 90 °N and joined together to create the two-dimensional matrix (time versus latitude) of mole fractions.

FTIR column observations.

FTIR total and partial column data were derived from ongoing Network for the Detection of Atmospheric Composition Change (NDACC, www.ndacc.org) observations from solar viewing FTIR instruments. The network instruments are calibrated to common standards to ensure consistent optical performance across the network and over time. High-resolution mid-infrared solar radiation is recorded on a near daily basis. Analyses of the JFJ ethane retrieval and time series are presented in ref. 12. An improved retrieval approach delivers enhanced information content and sensitivity up to ~20 km altitude, providing two independent partial column time series, for the 3.58–8 and 8–21 km altitude. The ethane retrieval used for the Lauder spectra is presented in ref. 45. Initial analyses of Lauder time series are described in ref. 46, where SH decreasing trends are given up to 2009. The statistical bootstrap resampling tool used for the trend calculations is presented in ref. 47. It determines a linear trend and corresponding uncertainties, and accounts for the seasonal/intra-annual variability of the data. Determination of the uncertainty in the ethane column trend of the JFJ time series is explained in ref. 12. Several settings were tried (that is, adjusting the step and integration interval) for the running mean calculations at JFJ and other NH FTIR sites (for example, Toronto), always coming up with an ethane trend reversal date close to late 2008–early 2009.

Emissions inventory.

The ethane emissions inventory is a best estimate based on three different resources that build on other previous inventories and publications. On the basis of reconstructed ambient air histories, a year 2000 global ethane emission was estimated at 8–10 Tg yr^{-1} (ref. 1). These authors do not differentiate between NH and SH emissions. Approximately 85% of ethane is estimated to be emitted in the NH (see (2) and (3) below). Based on that the global estimate translates to 7–9 Tg yr^{-1} of NH ethane emissions. Second, we evaluated the inventory developed for the Hemispheric Transport of Air Pollutants, Phase II (HTAP2), which is a composite of regional inventories harmonized to represent 2008 and 2010[48] emissions. Additional ethane emissions included in these simulations are biogenic emissions from the MEGAN2.1 (ref. 49), and fire emissions from FINNv1.5 (ref. 50). Simulations with CAM-chem indicated that the anthropogenic emissions needed to be doubled to match the pre-2009 NMHC FTIR observations at JFJ. A summary of

these adjusted emissions by region and sources is given in Supplementary Table 4 for 2007. Year 2009.5 NH ethane emissions are estimated as 15 Tg yr^{-1} from the 'Globe—all' minus the SH emissions. For a third resource, we used the RCP85 database (Representative Concentration Pathway 8.5)[51,52]. It includes total emissions of ethane of ~12.9 Tg yr^{-1}, of which 0.53, 2.3 and 10 Tg yr^{-1} are emitted from biogenic, biomass burning, and anthropogenic sources, respectively. Of the total 12.9 Tg yr^{-1}, 9.9 Tg yr^{-1} are emitted in the NH.

We used 9.9 Tg yr^{-1}, which is the middle value of these three estimates for the ethane, NMHC, and methane emission increase, and ozone sensitivity modelling, and 1/2 of the minimum (7 Tg yr^{-1}) to maximum (15 Tg yr^{-1}) range as the uncertainty interval (4 Tg yr^{-1}).

Scaling of methane to ethane.

The methane/ethane emission ratio was determined as the median of available data from analyses of both compounds in USA O&NG regions (Supplementary Table 5). We used 1/2 of the difference between the minimum and maximum value in the data as the uncertainty interval (5.6). The methane emission estimation uncertainty interval was calculated by error propagation including uncertainties in the ethane growth rate, the ethane inventory emission, and the methane/ethane ratio.

Scaling of total NMHC to ethane calculation.

There are few publications that report speciated NMHCs, and there are even fewer that include ethane, from O&NG source regions. Furthermore, some of the available literature studies suffer from measurements being influenced to a variable degree by other contributing sources. We compiled published speciated NMHC/ethane emission ratios from O&NG development areas in Supplementary Table 6. Ambient air measurements were converted to relative mass emission ratios scaled to ethane. The contribution of missing NMHC to the total NMHC emission > C_2 was estimated by adding up the relative fractions of missing species reported in the ref. 53 study and pro-rating the contribution of the missing species. There is a considerable amount of variability in these data, probably caused by the different NMHC emission ratios in different shale regions.

Among these data sets results from the Uintah Basin are likely to be of a relatively high representativeness for several reasons. First, despite the Uintah Basin having a low population density, atmospheric VOCs have been found to be highly elevated, dominated by emission from O&NG operations. In 2013 the basin had an estimated 4,300 oil- and 6,900 gas-producing wells; therefore, emissions reflect a combination of both types of wells. Second, this data set is the average over two campaigns from two subsequent years. Third, measurements represent an overall high number of samples. Fourth, data are from surface and tethered balloon measurements from January to February, when relatively shallow boundary layer conditions prevailed, which fostered accumulation of nearby emissions[14].

The mean and median values for $\sum E_{NMHC>C_2}/E_{ethane}$ from these studies were calculated as 2.47 and 1.85, respectively, with the Uintah Basin result being the medium value. For the reasons detailed above, we chose a Uintah median $\Sigma E_{NMHC>C_2}/E_{ethane}$ value as scaling factor. The uncertainty of 1.4 was determined as 0.5 times the range of minimum to maximum scaling factors from individual studies. Uncertainty of the scaled total NMHC emission was calculated by error propagation.

Ozone modelling.

EMAC (ECHAM5/MESSy for atmospheric chemistry version 2.50[54]) was used to develop a first order of magnitude estimation of the impact of the emissions increase of simple NMHC on ozone formation. Although most of the added ethane flux is probably from the USA, other global regions may potentially have contributed to the flux increase. To reflect this uncertainty, we applied lower estimates for several of the applied variables. We did not consider an increase in methane emissions on ozone production. We considered only estimated associated emissions of C_2–C_5, excluding NMHC > C_5, which constitute ~10% of the total O&NG NMHC emission (Supplementary Table 6), and on average have higher reactivity and ozone production potential than the lighter NMHC. Furthermore, the scaling value applied here is below the mean of available observations (Supplementary Table 6). The applied ethane NH inventory flux of 9.9 Tg yr^{-1} is a significantly lower value compared with the most recent estimate (15 Tg yr^{-1}, as explained above and in ref. 24). The model set-up was the same as in ref. 55, with the only exception of an augmented chemical scheme, which includes oxidation chemistry of

simple C_4–C_5 hydrocarbons (that is, *n*- and *iso*-butane, and *n*- and iso-pentane). The model simulations adopted emissions from the RCP85 database (Representative Concentration Pathway 8.5)[51,52]. Two simulations were performed for 2009.5–2014.5: one with constant NMHC emissions, named CONST, and the other with increasing NMHC, named TREND. To disentangle the impact of increased NMHC emissions, all other tracer emissions were kept constant. We applied a trend of 4.2% yr^{-1} for the NH emissions of ethane over five years based on the JFJ FTIR mid-troposphere column trend value. In the model NH emissions of ethane are ~9.9 Tg yr^{-1}, of which 0.17, 0.9, and 8.8 Tg yr^{-1} are emitted from biogenic, biomass burning and anthropogenic sources, respectively. Therefore, the ethane growth rate accounts to an increase in ethane emission O&NG sources of ~0.41 Tg yr^{-1}. Based on observed ambient air relative ratios of NMHC in source regions, see Supplementary Table 6, 0.30, 0.11, 0.08, 0.05 and 0.06 Tg yr^{-1} increases were prescribed to propane, *n*-butane, *iso*-butane, *n*-pentane, and iso-pentane, every year for five years, so that after five years the total emission increase was five times these listed emissions. Uncertainties in all scaling ratios propagate into the calculated ozone changes. The emissions map was based on shale O&NG wells distribution, available at http://frack.skytruth.org. Information used for generating this map is based on 'voluntary disclosure reports submitted by oil and gas drilling operators' and relies on locations of more than 15,000 wells. We assumed that all wells emit the same amounts of NMHC, neglecting difference in wells size and leakage rate. Finally, the distributed map of the wells was aggregated in a 0.5 × 0.5° regular map, and emissions were scaled on the basis of the well number density in each grid cell. The resulting emissions map (see Supplementary Fig. 1) identifies regions that have experienced recent growth of O&NG development, with regions of large emission increases in the central and northeastern USA.

Modelling results in Fig. 4 show the differences in the ozone molar fraction between model results from the simulation CONST and TREND. Note that these results are based on constant emissions of other precursors, including those of nitrogen oxides (NO_x). Decreasing trends of NO_x over the USA and of VOCs in urban areas have led to a general decrease of ozone in many urban regions. Omission of these effects will cause a high bias of the ozone changes that were calculated here. Consequently, these model results should be considered as preliminary results, providing an indication of the direction of

ozone effects from added O&NG emissions, and taken as motivation for more in-depth modelling of the net effect resulting from these emission changes.

Data availability.

The NMHC surface data used for this research are available at http://www.esrl.noaa.gov/gmd/dv/data and http://ds.data.jma.go.jp/gmd/wdcgg. The FTIR column observations can be retrieved from ftp://ftp.cpc.ncep.noaa.gov/ndacc/station.

References

1. Aydin, M. *et al.* Recent decreases in fossil-fuel emissions of ethane and methane derived from firn air. *Nature* **476**, 198–201 (2011).

2. Worton, D. R. *et al.* Evidence from firn air for recent decreases in non-methane hydrocarbons and a 20th century increase in nitrogen oxides in the northern hemisphere. *Atmos. Environ.* **54**, 592–602 (2012).

3. Helmig, D. *et al.* Reconstruction of Northern Hemisphere 1950–2010 atmospheric non-methane hydrocarbons. *Atmos. Chem. Phys.* **14**, 1463–1483 (2014).

4. Nicewonger, M. R., Verhulst, K. R., Aydin, M. & Saltzman, E. S. Preindustrial atmospheric ethane levels inferred from polar ice cores: a constraint on the geologic sources of atmospheric ethane and methane. *Geophys. Res. Lett.* **43**, 214–221 (2015).

5. Von Schneidemesser, E., Monks, P. S. & Plass-Duelmer, C. Global comparison of VOC and CO observations in urban areas. *Atmos. Environ.* **44**, 5053–5064 (2010).

6. Warneke, C. *et al.* Multiyear trends in volatile organic compounds in Los Angeles, California: five decades of decreasing emissions. *J. Geophys. Res.* **117**, D00V17 (2012).

7. Simpson, I. J. *et al.* Long-term decline of global atmospheric ethane concentrations and implications for methane. *Nature* **488**, 490–494 (2012).

8. Kramer, L. J. *et al.* Seasonal variability of atmospheric nitrogen oxides and non-methane hydrocarbons at the GEOSummit station, Greenland. *Atmos. Chem. Phys.* **12**, 6827–6849 (2015).

9. Plass-Duelmer, C., Michl, K., Ruf, R. & Berresheim, H. C_2–C_8 hydrocarbon measurement and quality control procedures at the Global Atmosphere Watch Observatory Hohenpeissenberg. *J. Chrom.* **953**, 175–197 (2002).

10. Read, K. A. *et al.* Intra-annual cycles of NMVOC in the tropical marine boundary layer and their use for interpreting seasonal variability in CO. *J. Geophys. Res.* **114**, D21303 (2009).

11. Leuchner, M. *et al.* Can positive matrix factorization help to understand patterns of organic trace gases at the continental Global Atmosphere Watch site Hohenpeissenberg? *Atmos. Chem. Phys.* **15**, 1221–1236 (2015).

12. Franco, B. *et al.* Retrieval of ethane from ground-based FTIR solar spectra using improved spectroscopy: recent burden increase above Jungfraujoch. *J. Quant. Spec. Radiat. Trans.* **160**, 36–49 (2015).

13. Pétron, G. *et al.* Hydrocarbon emissions characterization in the Colorado Front Range: a pilot study. *J. Geophys. Res.* **117**, 1–19 (2012).

14. Helmig, D. *et al.* Highly elevated atmospheric levels of volatile organic compounds in the Uintah Basin, Utah. *Environ. Sci. Technol.* **48**, 4707–4715 (2014).

15. Thompson, C. R., Hueber, J. & Helmig, D. Influence of oil and gas emissions on ambient atmospheric non-methane hydrocarbons in residential areas of Northeastern Colorado. *Elementa* **2**, 1–16 (2014).

16. Swarthout, R. F. *et al.* Impact of marcellus shale natural gas development in southwest Pennsylvania on volatile organic compound emissions and regional air

quality. *Environ. Sci. Technol.* **49**, 3175–3184 (2015).

17. Karion, A. *et al.* Methane emissions estimate from airborne measurements over a western United States natural gas field. *Geophys. Res. Lett.* **40**, 4393–4397 (2013).

18. Schnell, R. C. *et al.* Rapid photochemical production of ozone at high concentrations in a rural site during winter. *Nature Geosci.* **2**, 120–122 (2009).

19. Oltmans, S. *et al.* Anatomy of wintertime ozone associated with oil and natural gas extraction activity in Wyoming and Utah. *Elementa* **2**, 1–15 (2014).

20. Vinciguerra, T. *et al.* Regional air quality impacts of hydraulic fracturing and shale natural gas activity: evidence from ambient VOC observations. *Atmos. Environ.* **110**, 144–150 (2015).

21. Schade, G. W. & Roest, G. S. Is the shale boom reversing progress in curbing ozone pollution? *EOS* **96**, http://dx.doi.org.offcampus.lib.washington.edu/10.1029/2015EO028279 (2015).

22. *US Greenhouse Gas Inventory* (EPA, accessed 4 April, 2016); https://www3-epa-gov.offcampus.lib.washington.edu/climatechange/ghgemissions/index.html

23. Kirschke, S. *et al.* Three decades of global methane sources and sinks. *Nature Geosci.* **6**, 813–823 (2013).

24. Franco, B. *et al.* Evaluating ethane and methane emissions associated with the development of oil and natural gas extraction in North America. *Environ. Res. Lett.* **11**, 044010 (2016).

25. Hausmann, P., Sussmann, R. & Smale, D. Contribution of oil and natural gas production to renewed increase of atmospheric methane (2007–2014): top-down estimate from ethane and methane column observations. *Atmos. Chem. Phys.* **16**, 3227–3244 (2016).

26. Turner, A. J. *et al.* A large increase in US methane emissions over the past decade inferred from satellite data and surface observations. *Geophys. Res. Lett.* **43**, 2218–2224 (2016).

27. Schaefer, H. *et al.* A 21st century shift from fossil-fuel to biogenic methane emissions indicated by $^{13}CH_4$. *Science* http://dx.doi.org.offcampus.lib.washington.edu/10.1126/science.aad2705 (2016).

28. Peischl, J. *et al.* Quantifying atmospheric methane emissions from the Haynesville, Fayetteville, and northeastern Marcellus shale gas production regions. *J. Geophys. Res.* **120**, 2119–2139 (2015).

29. Karion, A. *et al.* Aircraft-based estimate of total methane emissions from the Barnett Shale region. *Environ. Sci. Technol.* **49**, 8124–8131 (2015).

30. Petron, G. *et al.* A new look at methane and nonmethane hydrocarbon emissions from oil and natural gas operations in the Colorado Denver-Julesburg Basin. *J. Geophys. Res.* **119**, 6836–6852 (2014).

31. Pollmann, J. *et al.* Sampling, storage, and analysis of C_2–C_7 non-methane hydrocarbons from the US National Oceanic and Atmospheric Administration Cooperative Air Sampling Network glass flasks. *J. Chromatogr. A* **1188**, 75–87 (2008).

32. Helmig, D. *et al.* Volatile organic compounds in the global atmosphere. *Eos Trans. AGU* **90**, 513–514 (2009).

33. *World Calibration Centre for Volatile Organic Compounds* (WCC-VOC) (Karlsruhe Institute of Technology, accessed 14 April 2016); http://www.imk-ifu.kit.edu/wcc-voc

34. *A WMO/GAW Expert Workshop on Global Long-Term Measurements of Volatile Organic Compounds* (VOCs) Report No. 171 36 (WMO, 2007).

35. Pollmann, J., Helmig, D., Hueber, J., Tanner, D. & Tans, P. P. Evaluation of solid adsorbent materials for cryogen-free trapping—gas chromatographic analysis of

atmospheric C_2–C_6 non-methane hydrocarbons. *J. Chromatogr. A* **1134**, 1–15 (2006).

36. *Global Atmospheric VOC Monitoring Program* (Atmospheric Research Laboratory, Institute of Arctic and Alpine Research, University of Colorado, accessed 31 March 2016); http://instaar.colorado.edu/arl/Global_VOC.html

37. Helmig, D., Stephens, C. R., Caramore, J. & Hueber, J. Seasonal behavior of non-methane hydrocarbons in the firn air at Summit, Greenland. *Atmos. Environ.* **85**, 234–246 (2014).

38. Miller, B. R. *et al.* Medusa: a sample preconcentration and GC/MS detector system for *in situ* measurements of atmospheric trace halocarbons, hydrocarbons, and sulfur compounds. *Anal. Chem.* **80**, 1536–1545 (2008).

39. Rhoderick, G. C. *et al.* International comparison of a hydrocarbon gas standard at the picomol per mol level. *Anal. Chem.* **86**, 2580–2589 (2014).

40. Thoning, K. W., Tans, P. P. & Komhyr, W. D. Atmospheric carbon-dioxide at Mauna Loa observatory.2. analysis of the NOAA GMCC data, 1974–1985. *J. Geophys. Res.* **94**, 8549–8565 (1989).

41. Yue, S., Pilon, P. & Cavadias, G. Power of the Mann-Kendall and Spearman's rho tests for detecting monotonic trends in hydrological series. *J. Hydrol.* **259**, 254–271 (2002).

42. Masarie, K. A. & Tans, P. P. Extension and integration of atmospheric carbon-dioxide data into a globally consistent measurement record. *J. Geophys. Res.* **100**, 11593–11610 (1995).

43. *GLOBALVIEW* (NOAA Earth System Research Laboratory Global Monitoring Division, accessed 4 April 2016), http://www.esrl.noaa.gov/gmd/ccgg/globalview

44. Tans, P. P., Conway, T. J. & Nakazawa, T. Latitudinal distribution of the sources and sinks of atmospheric carbon-dioxide derived from surface observations and an atmospheric transport model. *J. Geophys. Res.* **94**, 5151–5172 (1989).

45. Rinsland, C. P. *et al.* Multiyear infrared solar spectroscopic measurements of HCN, CO, C_2H_6, and C_2H_2 tropospheric columns above Lauder, New Zealand (45 °S latitude). *J. Geophys. Res.* **107**, ACH 1-1–ACH 1-12 (2002).

46. Zeng, G. *et al.* Trends and variations in CO, C_2H_6, and HCN in the Southern Hemisphere point to the declining anthropogenic emissions of CO and C_2H_6. *Atmos. Chem. Phys.* **12**, 7543–7555 (2012).

47. Gardiner, T. *et al.* Trend analysis of greenhouse gases over Europe measured by a network of ground-based remote FTIR instruments. *Atmos. Chem. Phys.* **8**, 6719–6727 (2008).

48. Janssens-Maenhout, G. *et al.* HTAP_v2: a mosaic of regional and global emission gridmaps for 2008 and 2010 to study hemispheric transport of air pollution. *Atmos. Chem. Phys.* **15**, 12867–12909 (2015).

49. Guenther, A. B. *et al.* The Model of Emissions of Gases and Aerosols from Nature version 2.1 (MEGAN2.1): an extended and updated framework for modeling biogenic emissions. *Geosci. Model Dev.* **5**, 1471–1492 (2012).

50. Wiedinmyer, C. *et al.* The Fire INventory from NCAR (FINN): a high resolution global model to estimate the emissions from open burning. *Geosci. Model Dev.* **4**, 625–641 (2011).

51. Riahi, K., Grübler, A. & Nakicenovic, N. Scenarios of long-term socio-economic and environmental development under climate stabilization. *Technol. Forecast. Soc. Change* **74**, 887–935 (2007).

52. Pozzer, A. *et al.* AOD trends during 2001–2010 from observations and model simulations. *Atmos. Chem. Phys.* **15**, 5521–5535 (2015).

53. Swarthout, R. F., Russo, R. S., Zhou, Y., Hart, A. H. & Sive, B. C. Volatile organic compound distributions during the NACHTT campaign at the Boulder Atmospheric Observatory: influence of urban and natural gas sources. *J. Geophys. Res.* **118**, 10614–10637 (2013).

54. Jöckel, P. *et al.* Development cycle 2 of the modular earth submodel system (MESSy2). *Geosci. Model Dev.* **3**, 717–752 (2010).

55. Pozzer, A. *et al.* Observed and simulated global distribution and budget of atmospheric C_2-C_5 alkanes. *Atmos. Chem. Phys.* **10**, 4403–4422 (2010).

Acknowledgements

This research would not have been possible without the contributions of many dedicated researchers that maintain the sampling programmes that provided the used data. The global VOC flask analyses are a component of NOAA's Cooperative USA- and global-scale Greenhouse Gas Reference flask sampling network, which is supported in part by NOAA Climate Program Office's AC4 Program. We greatly appreciate the work of many colleagues who have contributed to the programme operation and data processing, in particular C. Siso, P. Lang, J. Higgs, M. Crotwell, S. Wolter, D. Neff, J. Kofler, A. Andrews, B. Miller, D. Colegrove, C. Sweeney, E. Dlugokencky, and Y. Stenzel, and many unnamed CU Boulder undergraduate students who have processed the flask network data. The *in situ* monitoring at Summit is funded by the USA National Science Foundation, grant PLR-AON 1108391. We thank M. Fischer and S. Biraud for the operation of the STR and SGP site, respectively. The WGC and STR sites are operated with support from the California Energy Commission's Natural Gas programme under USA Department of Energy Contract No. DE-AC02-05CH11231. Financial support for the measurements at JFJ is provided by the International Foundation High Altitude Research Stations JFJ and Gornergrat (HFSJG), and for the GC/MS measurements also by the Swiss Federal Office for the Environment (FOEN) in the Swiss National Program HALCLIM. *In situ* VOC measurements at Cape Verde are made with the assistance of L. Mendes, K. Read, and J. Hopkins. The University of York thanks NCAS and NERC for funding. The FTIR measurements at NIWA, Lauder, are core funded through New Zealand's Ministry of Business, Innovation, and Employment. J.W.H. is supported by NASA under contract No. NNX13AH87G. The National Center for Atmospheric Research is supported by the USA National Science Foundation. The University of Liège contribution has been primarily supported by BELSPO and the

F.R.S.—FNRS (Fonds de la Recherche Scientifique), both in Brussels. We thank P. Martinerie, at LGGE, Grenoble, France, for the reconstructed ethane firn air history in Fig. 1a. The global VOC monitoring is under the auspices of the World Meteorological Organization Global Atmospheric Watch (WMO-GAW) programme, which facilitates coordination between participating partners and quality control efforts. The VOC World Calibration Centre is funded by the German Umweltbundesamt. We also thank the staff of the World Data Centre for Greenhouse Gases at the Japan Meteorological Agency for the archiving and public posting of data used in this study.

Author information

Affiliations

Institute of Arctic and Alpine Research, University of Colorado, Boulder, Colorado 80305, USA
Detlev Helmig, Samuel Rossabi & Jacques Hueber

Earth Systems Research Laboratory, National Oceanic and Atmospheric Administration, Boulder, Colorado 80305, USA
Pieter Tans, Stephen A. Montzka, Ken Masarie & Kirk Thoning

Deutscher Wetterdienst, 82383 Hohenpeissenberg, Germany
Christian Plass-Duelmer & Anja Claude

Wolfson Atmospheric Chemistry Laboratories, University of York, York YO10 5DD, UK
Lucy J. Carpenter & Shalini Punjabi

National Centre for Atmospheric Science, University of York, York YO10 5DD, UK
Alastair C. Lewis

Laboratory for Air Pollution and Environmental Technology, Empa, Swiss Federal Laboratories for Materials Science and Technology, 8600 Duebendorf, Switzerland
Stefan Reimann & Martin K. Vollmer

Karlsruhe Institute for Technology, Campus Alpine, 82467 Garmisch-Partenkirchen, Germany

Rainer Steinbrecher

National Center for Atmospheric Research, Boulder, Colorado 80301, USA
James W. Hannigan & Louisa K. Emmons

Institute of Astrophysics and Geophysics, University of Liège, 4000 Liège, Belgium
Emmanuel Mahieu & Bruno Franco

National Institute of Water and Atmospheric Research, Lauder 9352, New Zealand
Dan Smale

Max Planck Institute for Chemistry, 55128 Mainz, Germany
Andrea Pozzer

Contributions

D.H., study design, global flask network operation, Summit *in situ* measurements, data analyses, quality control, site comparisons, manuscript preparation. S.R., data processing, preparation of graphs, manuscript preparation. J.H., global flask network operation, analytical work, Summit *in situ* measurements. P.T., global flask network operation, manuscript preparation. S.A.M., propane data from the North American Tower flask programme and its quality control, manuscript preparation. K.M., NOAA network data management, NMHC global graphs shown in Fig. 2, manuscript preparation. K.T., data filtering, trend analyses, data statistics, manuscript preparation. C.P.-D., HPB NMHC monitoring, flask–*in situ* comparisons, manuscript preparation. A.C., HPB *in situ* NMHC monitoring. A.C.L., CVO NMHC *in situ* observations, manuscript preparation. L.J.C., CVO NMHC *in situ* observations, manuscript preparation. S.P., CVO NMHC *in situ* observations. S.R., JFJ NMHC *in situ* observations. M.K.V., JFJ NMHC *in situ* observations, manuscript preparation. R.S., VOC World Calibration Center, NMHC quality control, manuscript preparation. J.W.H., FTIR data evaluations and coordination, manuscript preparation. L.K.E., emissions modelling, ethane inventory data, manuscript preparation. E.M., JFJ FTIR data processing and analyses, manuscript preparation. B.F., JFJ FTIR data processing and analyses, manuscript preparation. D.S., Lauder FTIR observations and data processing, manuscript preparation. A.P., ethane inventory data, photochemical ozone modelling, manuscript preparation.

Competing interests

The authors declare no competing financial interests.

Corresponding author

Correspondence to Detlev Helmig.

Supplementary information

PDF files

1. Supplementary Information
   Supplementary Information

Nature Geoscience ISSN 1752-0908 (online)